

000 001 002 003 004 005 006 007 008 009 010 011 012 013 014 015 016 017 018 019 020 021 022 023 024 025 026 027 028 029 030 031 032 033 034 035 036 037 038 039 040 041 042 043 044 045 046 047 048 049 050 051 052 053 KEYSYNC: A ROBUST APPROACH FOR LEAKAGE-FREE LIP SYNCHRONIZATION IN HIGH RESOLUTION

Anonymous authors

Paper under double-blind review

ABSTRACT

Lip synchronization, known as the task of aligning lip movements in an existing video with new input audio, is typically framed as a simpler variant of audio-driven facial animation. However, as well as suffering from the usual issues in talking head generation (e.g., temporal consistency), lip synchronization presents significant new challenges such as expression leakage from the input video and facial occlusions, which can severely impact real-world applications like automated dubbing, but are largely neglected by existing works. To address these shortcomings, we present KeySync, a two-stage framework that succeeds in solving the issue of temporal consistency, while also incorporating solutions for leakage and occlusions using a carefully designed masking strategy. We show that KeySync achieves state-of-the-art results in lip reconstruction and cross-synchronization, improving visual quality and reducing expression leakage according to LipLeak, our novel leakage metric. Furthermore, we demonstrate the effectiveness of our new masking approach in handling occlusions and validate our architectural choices through several ablation studies. Our code and models will be made publicly available.

1 INTRODUCTION

Audio-driven facial animation has recently seen substantial progress with the introduction of new generative models such as Generative Adversarial Networks (GANs) Goodfellow et al. (2020); Vougioukas et al. (2019); Zhou et al. (2019) and diffusion models Ho et al. (2020); Stypulkowski et al. (2024); Chen et al. (2024b). In contrast, the adjacent field of lip synchronization (also known as lip-sync) has experienced comparatively slower advancements Guan et al. (2023); Zhang et al. (2023d); Prajwal et al. (2020). This disparity is surprising given that lip-sync has similar applications, ranging from facilitating multilingual content production to enhancing virtual avatars Zhen et al. (2023); Zhan et al. (2023). A potential reason for this slower progress is that while lip synchronization may seem like a simpler task than animating the full face from audio, it presents unique challenges that remain largely unaddressed.

Current methods are limited in both visual quality and temporal consistency. Most models are constrained to a low-resolution (256×256) output, hindering real-world applicability. Furthermore, they struggle with temporal stability; frame-based approaches Yu et al. (2024); Liu et al. (2024) often produce visible discontinuities, while attempts to enforce coherence indirectly through perceptual models Li et al. (2024), sequence discriminators Mukhopadhyay et al. (2024), or autoregressive conditioning Bigioi et al. (2024) can introduce subtle artifacts or suffer from error accumulation over long sequences.

Beyond temporal consistency, a key, but often overlooked issue is expression leakage, where models infer mouth shapes from facial expressions in the source video rather than from the driving audio. Regrettably, most existing works focus excessively on lip synchronization as a reconstruction task on paired audio-visual data, and neglect the cross-synchronization scenario, where a non-matching audio clip is used to re-animate the original video. As a consequence, they typically exhibit major expression leakage from the original video, severely degrading the synchronization between the generated video and the input audio in the latter scenario. Notably, this behaviour jeopardizes the viability of these models for applications like automated dubbing, where audio and video are naturally mismatched.

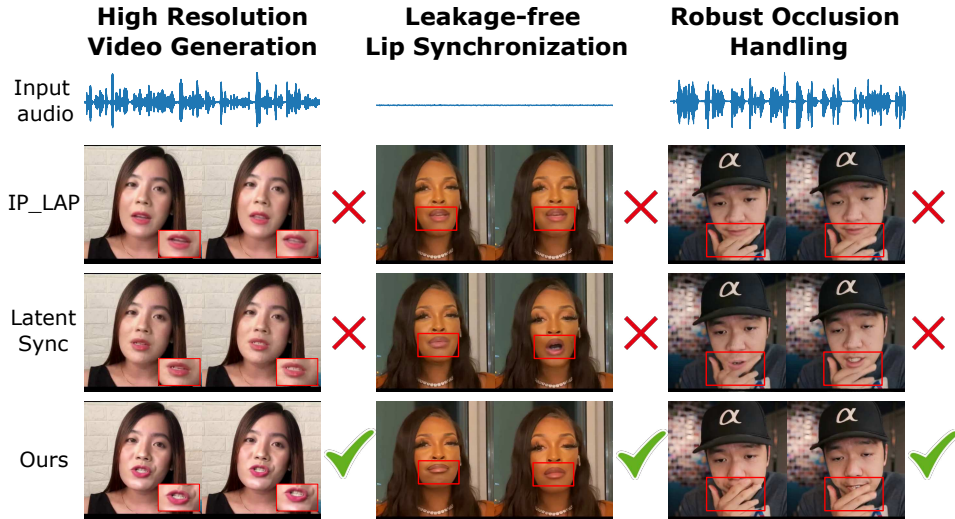


Figure 1: Unlike existing methods, KeySync generates high-resolution lip-synced videos that are closely aligned with the driving audio while minimizing leakage from the input video and seamlessly handling facial occlusions.

To alleviate expression leakage, some methods Cheng et al. (2022); Yaman et al. (2024) introduce an additional network to generate a neutral version of the input frame, neglecting the underlying issue of the masking strategy. Some methods mask only the mouth region while preserving facial areas such as the jaw and cheeks from the original videos, potentially leading to leakage since these regions also convey information about mouth movements Ki & Min (2023); Zhang et al. (2023d), while others adopt broader masks that risk discarding important contextual cues Zhang et al. (2024); Cheng et al. (2022). Remarkably, the impact of these masking strategies on generalization and robustness remains largely unexplored, and no consensus exists on the optimal approach. Lastly, another potential complication lies in occlusion handling. Most existing models assume an unobstructed view of the mouth, whereas, in the real world, occlusions caused by hands, objects, or motion blur are frequent. In practice, this means that the lack of explicit occlusion-handling mechanisms significantly limits the applicability of current models.

To address these challenges, we propose KeySync, a two-stage lip synchronization framework that leverages recent advances in facial animation to generate high-fidelity videos with lip movements that are temporally consistent and aligned with the input audio. To minimize leakage from the input video, we devise a masking strategy that adequately covers the lower face while retaining the necessary contextual regions. Furthermore, we augment this mask by excluding facial occlusions using a video segmentation model, resulting in a method that consistently handle occlusions without uncanny visual hallucinations. Our primary contributions, illustrated in Figure 1, are:

- **State-of-the-art lip synchronization:** KeySync achieves state-of-the-art lip synchronization performance at a resolution of (512×512) , surpassing the common (256×256) standard. It outperforms all competing methods in terms of quality and lip movement accuracy according to several objective metrics and a holistic user study. We observe particularly noticeable improvements in the cross-synchronization setting (where there is a mismatch between the input video and audio), enabling promising real-world applications such as automated dubbing.
- **A new strategy for occlusion handling:** We propose an inference-time strategy for occlusion handling by excluding occluding objects from our mask automatically using a pre-trained video segmentation model. Through qualitative and quantitative analysis, we show this method is consistently effective in handling occlusions.
- **A novel leakage metric:** We propose LipLeak, the first metric to quantify lip synchronization leakage. It measures how much motion from the source video leaks into the output by computing the ratio in lip activity between videos generated using speech versus silent audio.

108 **2 RELATED WORKS**

110 **Audio-Driven Facial Animation** Audio-driven facial animation methods aim to generate realistic
 111 talking head videos with accurate lip-sync and preserved identity. Early GAN-based works Vou-
 112 gioukas et al. (2019); Zhou et al. (2019); Chung et al. (2017) focused on lip-sync, while later ap-
 113 proaches incorporated head pose modelling but often introduced artifacts and unnatural motion Chen
 114 et al. (2020); Zhang et al. (2023c); Zhou et al. (2021).

115 Diffusion models Ho et al. (2020); Rombach et al. (2022) have since emerged as a superior alter-
 116 native, demonstrating improved temporal consistency and video quality Xu et al. (2024b). Several
 117 modern methods leverage video diffusion models for temporally consistent motion Stypulkowski
 118 et al. (2024); Xu et al. (2024a). Others condition the generation process on facial landmarks Wei
 119 et al. (2024) or 3D meshes Zhang et al. (2023a); however, these approaches often produce unreal-
 120 istic facial motion. To improve identity reconstruction, recent works Chen et al. (2024b); Xu et al.
 121 (2024a) leverages ReferenceNet Hu (2024), though at the cost of increased computational complex-
 122 ity. However, these state-of-the-art methods, including recent keyframe-based techniques Bigata
 123 et al. (2025), are designed for full-face generation. Our work addresses the distinct challenge of
 124 lip-sync editing, which involves unique problems such as expression leakage from the source video.

125 **Audio-Driven Lip Synchronization** Lip synchronization methods focus on adjusting mouth
 126 movements to match an audio input while preserving other facial attributes, such as head pose and
 127 upper face expressions. A foundational work, Wav2Lip Prajwal et al. (2020), uses a Generative
 128 Adversarial Network (GAN) to generate lip-synced frames, leveraging a pre-trained expert model
 129 to ensure accuracy. To enhance realism and identity generalization, subsequent methods have in-
 130 troduced StyleGAN2-based architectures Guan et al. (2023); Ki & Min (2023), spatial deformation
 131 of feature maps Zhang et al. (2023d), and coarse-to-fine pyramid models Muaz et al. (2023). Other
 132 approaches include LipFormer Wang et al. (2023b), which uses a codebook of face parts aligned
 133 with the audio, and TalkLip Zhong et al. (2023), which employs contrastive learning to improve the
 134 quality of the generated lip region. More recently, diffusion-based methods have been introduced
 135 for lip synchronization Mukhopadhyay et al. (2024); Liu et al. (2024); Bigioi et al. (2024), marking
 136 a shift in the state-of-the-art.

137 Despite these advances, several key challenges remain. The first is expression leakage, which is
 138 particularly problematic in cross-driving scenarios where one person’s expression is transferred to
 139 another. This leakage often stems from suboptimal masking strategies that fail to cover all visual
 140 cues of speech. While some methods Cheng et al. (2022); Yaman et al. (2024) address this by
 141 neutralizing the source face, this approach adds computational overhead and potential errors from
 142 the synthetic input. To date, no consensus exists on an optimal masking strategy.

143 A second challenge is temporal consistency. Many methods Yu et al. (2024); Liu et al. (2024);
 144 Zhong et al. (2024) operate on a frame-by-frame basis, leading to visible discontinuities. Models
 145 that condition on past frames Bigioi et al. (2024) can suffer from cumulative error propagation, while
 146 other techniques like perceptual models Li et al. (2024) or sequence discriminators Mukhopadhyay
 147 et al. (2024) are often insufficient to guarantee coherence.

148 Finally, occlusion handling remains a largely unsolved problem. Most models assume an unob-
 149 structed view of the mouth, failing in real-world settings with occlusions from hands, objects, or
 150 motion blur. Notably, Peng et al. (2025) propose a mask-free method lip sync method, which suc-
 151 ceeds in handling occlusions, but falls short in terms of lip synchronization.

152 **3 METHOD**

153 In this section, we describe our two-stage lip-sync approach, followed by our masking strategy in
 154 Section 3.2 and a new method for handling occlusions in Section 3.5.

155 **3.1 LATENT DIFFUSION**

156 Diffusion models Ho et al. (2020); Dhariwal & Nichol (2021) progressively transform random noise
 157 into structured data by iteratively removing noise through a learned denoising process. Latent diffu-
 158 sion Rombach et al. (2022) applies this denoising operation in a compressed latent space rather than

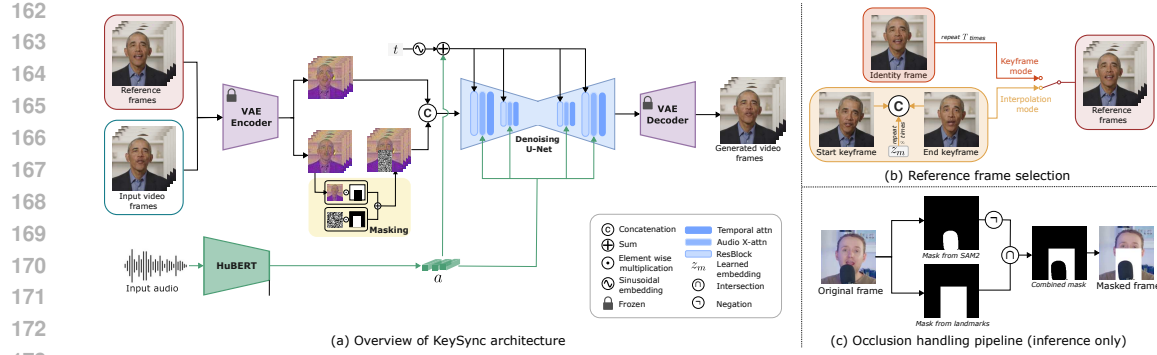


Figure 2: Overview of the KeySync framework. This two-stage latent diffusion model conditions on audio (a) and an input video. (b) The keyframe stage uses an identity frame z_{id} , while the interpolation stage uses keyframes (z_i, z_{i+1}) and intermediate embeddings (z_m). (c) Our inference-time occlusion handling pipeline.

in the high-dimensional pixel space, improving computational efficiency. Furthermore, the EDM framework Karras et al. (2022) defines the denoising operation of the denoiser D_θ as:

$$D_\theta(\mathbf{x}; \sigma) = c_{\text{skip}}(\sigma)\mathbf{x} + c_{\text{out}}(\sigma)F_\theta(c_{\text{in}}(\sigma)\mathbf{x}; c_{\text{noise}}(\sigma)), \quad (1)$$

where F_θ is the trainable neural network and \mathbf{x} the input. The terms $c_{\text{noise}}(\sigma)$, $c_{\text{out}}(\sigma)$, $c_{\text{skip}}(\sigma)$, and $c_{\text{in}}(\sigma)$ are scaling factors dependent on the noise level σ . These scaling factors dynamically adjust the magnitude and influence of noise at different stages of the denoising process, thereby improving the network's efficiency and robustness during diffusion.

3.2 LEAKAGE-PROOF MASKING

We frame the lip-sync task as a video inpainting problem Quan et al. (2024); Saharia et al. (2022) in the latent space. The critical objective is to ensure the newly generated lip region does not reuse (or “leak”) cues from the original mouth shape that contradict the new audio. Specifically, we create a mask M by computing facial landmarks Bulat & Tzimiropoulos (2017) and isolating the lower facial region, extending slightly above the nose to cover any upper cheek movements that could otherwise convey information about lip movements, while still preserving overall facial identity. The mask also extends to the lower edge of the image, preventing any leakage from jaw movements. We find that this mask strikes an appropriate balance, avoiding the excessive context loss of full lower-face masks Shen et al. (2023); Mukhopadhyay et al. (2024); Park et al. (2022) while preventing the expression leakage common with tight mouth-only masks Zhang et al. (2023d); Liu et al. (2024); Ki & Min (2023). While we group prior work into these two categories, it's important to note that each method implements its own masking strategy, and the exact details are not always shared. This highlights the need for a standardized approach. We provide pseudo-code to reproduce our mask and a deeper discussion on the topic in Appendix C.

3.3 TWO-STAGE VIDEO GENERATION

Our approach is illustrated in Figure 2. We follow the two-stage procedure of KeyFace Bigata et al. (2025) and adapt it to generate lip-synced animations from a masked input video and a driving audio clip. We feed the video frames $\{x_t\}_{t=1}^T$ into our VAE encoder Blattmann et al. (2023) \mathcal{V} to obtain latent representations $\{z_t\}_{t=1}^T$. We then add noise to obtain their corresponding noisy versions $\{z_t^n\}_{t=1}^T$. Then, using the predefined mask M , we define the input to the U-Net as:

$$z_t^m = M \odot z_t^n + (1 - M) \odot z_t, \quad (2)$$

where \odot denotes element-wise multiplication. We aim to generate video frames $\{\hat{x}_t\}_{t=1}^T$ where lip movements are synchronized with a given audio track $\{a_t\}_{t=1}^T$. Unlike previous approaches that either generate all frames end-to-end Ki & Min (2023); Wang et al. (2023a); Li et al. (2024) or explicitly disentangle motion and appearance Liu et al. (2024); Zhong et al. (2024); Yu et al. (2024), we ensure temporal continuity by separating the prediction of long-range motion (keyframes) from

short-range motion (interpolation). This approach allows us to model the video’s temporal dynamics directly without requiring auxiliary losses Mukhopadhyay et al. (2024), perceptual models Li et al. (2024), or motion-specific frames Bigioi et al. (2024).

	Method	CMMD \downarrow	TOPIQ \uparrow	VL \uparrow	FVD \downarrow	LipScore \uparrow	Lipleak \downarrow	Elo \uparrow
Reconstruction	DiffDub Liu et al. (2024)	0.403	0.44	37.12	429.07	0.34	-	1014
	IP_LAP Zhong et al. (2023)	<u>0.091</u>	<u>0.49</u>	37.77	<u>282.02</u>	0.36	-	1007
	Diff2Lip Mukhopadhyay et al. (2024)	0.225	0.48	35.84	555.08	0.49	-	886
	TalkLip Wang et al. (2023a)	0.230	0.39	29.07	608.92	0.58	-	920
	LatentSync Li et al. (2024)	0.319	0.41	45.23	343.90	0.52	-	1052
	KeySync	0.064	0.58	70.32	191.21	0.46	-	1120
Cross-sync	DiffDub Liu et al. (2024)	0.408	0.44	37.05	420.66	0.34	0.56	947
	IP_LAP Zhong et al. (2023)	<u>0.093</u>	0.49	35.32	<u>294.66</u>	0.17	0.57	1031
	Diff2Lip Mukhopadhyay et al. (2024)	0.231	<u>0.48</u>	33.97	601.68	0.16	0.42	878
	TalkLip Wang et al. (2023a)	0.201	0.42	24.80	704.93	0.30	0.90	911
	LatentSync Li et al. (2024)	0.325	0.41	45.95	361.57	0.14	0.64	1086
	KeySync	0.070	0.58	73.04	206.32	0.48	0.22	1145

Table 1: Quantitative comparison with other works on reconstruction and cross-synchronization performance. The best results are highlighted in **bold**, while the second-best results are underlined. All metrics are described in Section 4.2.

Architecture. Both stages share the Stable Video Diffusion (SVD) Blattmann et al. (2023) architecture. The input to each stage consists of reference frames, the target audio, and the original video frames. The reference frames serve to either condition the interpolation or preserve identity. We use HuBERT Hsu et al. (2021) to extract audio embeddings. These condition the model’s U-Net via cross-attention layers and timestep embeddings, enhancing video-audio alignment. Furthermore, we employ a modified classifier-free guidance strategy that decouples audio and identity conditions, which we found significantly boosts lip-synchronization accuracy (see Appendix H).

Keyframes. This stage generates a sparse set of keyframes, $\{\hat{x}_{t_k}\}_{k=1}^T$, where each keyframe is spaced S frames apart ($t_k = k \cdot S$). These keyframes serve as anchor points, ensuring that each one accurately reflects the phonetic content of the audio while preserving the subject’s identity. In this stage, the reference input consists of an identity frame, randomly sampled from the source video and repeated T times. To improve generalization, we augment these reference frames with noise Ho et al. (2022) and standard image augmentations.

Interpolation. This stage interpolates between successive keyframes to achieve smooth, coherent motion. The reference frames takes two consecutive keyframes in the latent space, \hat{z}_{t_i} and $\hat{z}_{t_{i+1}}$, and constructs the following input sequence to generate the intermediate frames:

$$s = \{z_{t_i}, \underbrace{z_m, \dots, z_m}_{\text{repeat } S \text{ times}}, z_{t_{i+1}}\}, \quad (3)$$

where z_m is a learnable embedding.

3.4 LOSSES

We adopt the loss formulation from Karras et al. 2022:

$$\mathcal{L}_{latent} = \mathbb{E}_{x,c,t,\sigma} \left[w_t \|F_\theta(z_t^m; c, \sigma_t) - z_t\|_2^2 \right], \quad (4)$$

where w_t is a weighting function, F_θ is the model, σ_t is the noise level, and c the conditioning inputs (audio and reference frames). We find that this loss alone is sufficient to achieve good lip synchronization and high-quality video generation. However, working solely in the compressed latent space can make it difficult for the model to retain fine semantic details Zhang et al. (2023b), which are critical for real-world lip synchronization tasks where preserving the nuances of the mouth region is essential. To address this, we introduce an additional L_2 loss in the RGB space. This requires decoding the latent output using the VAE decoder \mathcal{V} , resulting in:

$$\mathcal{L}_{rgb} = \mathbb{E}_{x,c,t,\sigma} \left[w_t \|\mathcal{V}(F_\theta(z_t^m; c, \sigma_t)) - x_t\|_2^2 \right]. \quad (5)$$

270 The final combined loss is then:
 271

$$\mathcal{L}_{total} = M \cdot \lambda(t)(\mathcal{L}_{latent}(\hat{z}, z) + \lambda_2 \mathcal{L}_{rgb}(\hat{x}, x)), \quad (6)$$

273 where $\lambda(t)$ is a weighting factor dependent on the diffusion timestep t , as defined in EDM Karras
 274 et al. (2022). Importantly, we ensure that only the generated region contributes to the loss computa-
 275 tion by masking the region of interest.
 276

277 3.5 HANDLING OCCLUSIONS

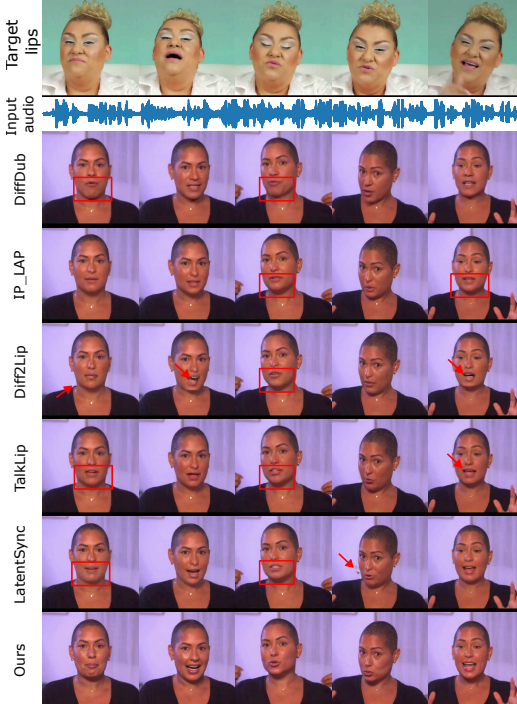
279 Occlusions are a critical yet often overlooked challenge in lip synchronization. Even advanced mod-
 280 els can produce unnatural results if occlusions in the original video, such as a hand or microphone
 281 covering the mouth, are not properly accounted for. A common issue arises when an occlusion
 282 overlaps with the mouth region during masking, often causing the model to incorrectly generate the
 283 mouth over the occluding object, resulting in unnatural boundary artifacts.
 284

285 To address this, we propose an inference-time solution to handle any occlusion without retraining.
 286 Explicitly training a model for occlusion handling is impractical due to the vast range of possible
 287 occlusions and their inherent misalignment with speech, making them hard for the model to learn.
 288 Instead, we introduce a preprocessing pipeline that first segments the occluding object using a state-
 289 of-the-art zero-shot video segmentation model Ravi et al. (2024), generating a mask M_{obj} of the
 290 occlusion. We then refine the original mask M by excluding the occlusion:
 291

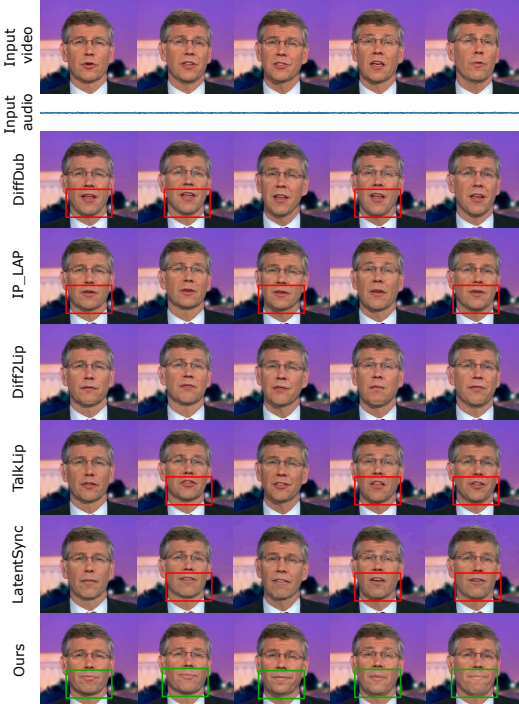
$$M' = M \cap \neg M_{obj}, \quad (7)$$

292 where \cap denotes intersection and \neg denotes logical negation. Since our model supports free-form
 293 masks, as in RePaint Lugmayr et al. (2022), it can seamlessly reconstruct the mouth region while
 294 preserving the occluding object, ensuring visually coherence.
 295

296 4 EXPERIMENTS



321 Figure 3: Qualitative comparison. “Target lips”
 322 (top row) shows the ground truth lip movements
 323 for the input audio.



321 Figure 4: Qualitative leakage comparison. We
 322 condition the models on silent audio and non-
 323 silent video (first row).
 324

324 4.1 DATASETS
325

326 We train on a combination of HDTF Zhang et al. (2021), CelebV-HQ Zhu et al. (2022), and CelebV-
327 Text Yu et al. (2023). To address artifacts in CelebV-HQ and CelebV-Text (e.g., low-quality, poor
328 framing), we developed a data curation pipeline, which is detailed in Appendix A.

329 For evaluation, we focus on the cross-sync task, the primary use case for lip-sync models, where
330 the input audio comes from a different video than the one being generated. We randomly select 100
331 test videos from CelebV-Text, CelebV-HQ, and HDTF and swap their audio tracks. Additionally, to
332 ensure consistency with prior works, we also report reconstruction results for the same 100 videos.
333

334 4.2 EVALUATION METRICS
335

336 We evaluate our method using a set of no-reference metrics. For image quality, we measure the
337 variance of Laplacian (VL) Pech-Pacheco et al. (2000) to assess blurriness, along with CMMD Jaya-
338 sumana et al. (2024), an improved version of FID, and a facial-domain TOPIQ Chen et al. (2024a);
339 Chen & Mo (2022). For video quality, we use FVD Unterthiner et al. (2019). For lip synchronization,
340 we rely on LipScore Bigata et al. (2025), which correlates better with human perception than
SyncNet LSE-C and LSE-D Chung & Zisserman (2016). We also introduce LipLeak, detailed be-
341 low, to quantify expression leakage. For completeness, SyncNet results are included in Appendix G.
342

343 **LipLeak** We introduce LipLeak to quantify expression leakage from a source video. We drive a
344 model with both speech and silent audio; since silent audio provides a zero-signal ground truth, any
345 resulting mouth motion is considered a leakage artifact. LipLeak is the ratio of the Mouth Aspect
346 Ratio (MAR) Kannan et al. (2023) standard deviation (σ) between the silent and speech-driven
347 outputs:

$$348 \text{LipLeak} = \frac{\sigma(MAR_{silence})}{\sigma(MAR_{speech}) + \epsilon}, \quad (8)$$

350 where ϵ ensures numerical stability. A low score is desirable, indicating expressive movement during
351 speech and stability during silence. Conversely, a high score signals a problem, diagnosable by
352 inspecting the components: a low $\sigma(MAR_{speech})$ suggests the model fails to generate expressive
353 motion for speech, while a high $\sigma(MAR_{silence})$ points to instability or leakage, which manifests as
354 unwanted mouth movement during silent periods. See Appendix D for further details.
355

356 4.3 USER STUDY
357

358 While the metrics above offer an objective evaluation, they do not always align with human per-
359 ception. To address this, we conduct a user study where participants compare randomly selected
360 video pairs based on lip synchronization, temporal coherence, and visual quality. We then rank the
361 performance of each model using the Elo rating system Elo (1978), and apply bootstrapping Chiang
362 et al. (2024) for robustness. Further details are provided in Appendix F.
363

364 5 RESULTS
365

366 This section presents a comprehensive evaluation of our model’s performance against baselines,
367 along with ablations to assess the impact of key components. Additional results are in Appendix G.
368

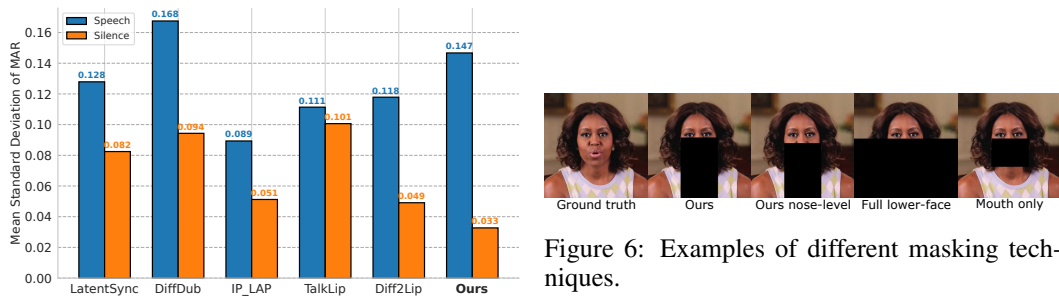
369 5.1 COMPARISON WITH OTHER WORKS
370

371 **Quantitative Analysis.** We evaluate our method alongside five competing approaches in Table 1.
372 The evaluation is conducted in two settings: reconstruction, where videos are generated using the
373 same audio as in the original video, and cross-sync, where the audio is taken from a different video.
374 The latter is particularly relevant as it better reflects real-world applications such as automated dub-
375 bing, where the driving audio is typically not aligned with the input video.

376 As shown in Table 1, KeySync achieves superior visual quality and temporal consistency (VL, FVD)
377 in both tasks. While most methods’ lip-sync quality (LipScore) degrades in the more challenging
cross-sync setting, our performance remains stable. Some baselines achieve a high LipScore in the

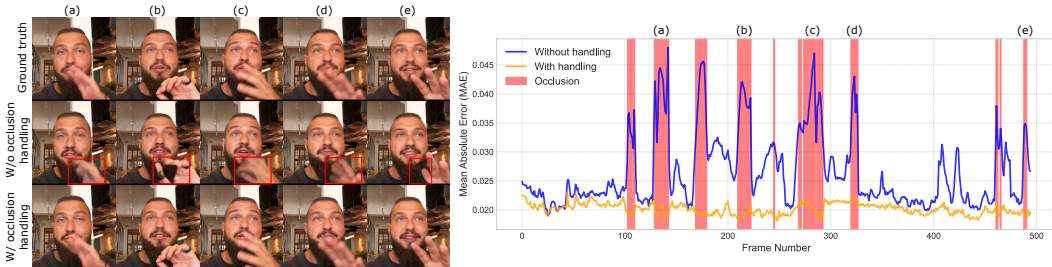
378 reconstruction task, but this is an artifact of expression leakage, confirmed by their high LipLeak
 379 scores. For instance, LipLeak reveals that DiffDub’s high cross-sync LipScore stems from random,
 380 unsynchronized mouth movements. Crucially, KeySync also obtains the highest Elo rating in our
 381 user study, confirming its state-of-the-art performance in human perception.
 382

383 **Qualitative Analysis.** Figure 3 shows a qualitative cross-sync comparison. KeySync more accu-
 384 rately follows the lip movements corresponding to the input audio. While LatentSync and Diff2Lip
 385 also appear to align somewhat with the target lip movements, they fail to generate certain vocal-
 386izations correctly and exhibit visual artifacts (highlighted on the figure via red squares and arrows,
 387 respectively), limiting their practical usability. Additionally, most methods produce insufficient
 388 mouth movement. This can be attributed to expression leakage, where conflicting signals from the
 389 source video and new audio hinder the generation of a coherent mouth region.
 390



401 Figure 5: We show the mean standard deviation
 402 of MAR for silent and speech audios.
 403

404 **Leakage.** As discussed in Section 4.2, we compute LipLeak by generating a video using a silent
 405 audio input. Since the audio contains no speech, the mouth should exhibit minimal movement.
 406 However, in practice, we observe this is not always the case, as expressions from the input video
 407 can leak into the generated output. Figure 4 shows qualitative examples where all methods, except
 408 ours and Diff2Lip, exhibit several frames where the mouth is open (highlighted by red squares) due
 409 to expression leakage. While Diff2Lip manages to keep the mouth closed, it introduces significant
 410 blending artifacts, highlighting the model’s struggle to suppress the original video’s motion. In
 411 Figure 5, we visualize the standard deviation of the Mouth Aspect Ratio (MAR) for both silent and
 412 speech audios. The results show that baselines either produce unwanted motion during silence (e.g.,
 413 DiffDub, LatentSync), suppressed motion during speech (e.g., IP_LAP), or similar motion in both
 414 cases (e.g., TalkLip). In contrast, KeySync exhibits the desired behavior: high motion variability for
 415 speech and minimal motion for silence, confirming its robustness against leakage.
 416



426 Figure 7: We present occlusion qualitative results on the left and quantitative results on the right.
 427

428 **Occlusion Handling.** Figure 7 demonstrates our method’s effectiveness. Without occlusion han-
 429 dling, significant artifacts appear around the hand (left), a finding confirmed by spikes in the mean
 430 absolute error plot (right). Our proposed method eliminates these artifacts by preserving the occlud-
 431 ing object while maintaining correct lip synchronization, resulting in a much lower reconstruction
 432 error. We assess this technique on baseline models in Appendix E.
 433

432 5.2 ABLATION STUDIES
433
434	435	436	437	438	439	440	441	442	443	444	445	446	447	448	449	450	451	452	453	454	455	456	457	458	459	460	461	462	463	464	465	466	467	468	469	470	471	472	473	474	475	476	477	478	479	480	481	482	483	484	485	486	487	488	489	490	491	492	493	494	495	496	497	498	499	500	501	502	503	504	505	506	507	508	509	510	511	512	513	514	515	516	517	518	519	520	521	522	523	524	525	526	527	528	529	530	531	532	533	534	535	536	537	538	539	540	541	542	543	544	545	546	547	548	549	550	551	552	553	554	555	556	557	558	559	560	561	562	563	564	565	566	567	568	569	570	571	572	573	574	575	576	577	578	579	580	581	582	583	584	585	586	587	588	589	590	591	592	593	594	595	596	597	598	599	600	601	602	603	604	605	606	607	608	609	610	611	612	613	614	615	616	617	618	619	620	621	622	623	624	625	626	627	628	629	630	631	632	633	634	635	636	637	638	639	640	641	642	643	644	645	646	647	648	649	650	651	652	653	654	655	656	657	658	659	660	661	662	663	664	665	666	667	668	669	670	671	672	673	674	675	676	677	678	679	680	681	682	683	684	685	686	687	688	689	690	691	692	693	694	695	696	697	698	699	700	701	702	703	704	705	706	707	708	709	710	711	712	713	714	715	716	717	718	719	720	721	722	723	724	725	726	727	728	729	730	731	732	733	734	735	736	737	738	739	740	741	742	743	744	745	746	747	748	749	750	751	752	753	754	755	756	757	758	759	760	761	762	763	764	765	766	767	768	769	770	771	772	773	774	775	776	777	778	779	780	781	782	783	784	785	786	787	788	789	790	791	792	793	794	795	796	797	798	799	800	801	802	803	804	805	806	807	808	809	810	811	812	813	814	815	816	817	818	819	820	821	822	823	824	825	826	827	828	829	830	831	832	833	834	835	836	837	838	839	840	841	842	843	844	845	846	847	848	849	850	851	852	853	854	855	856	857	858	859	860	861	862	863	864	865	866	867	868	869	870	871	872	873	874	875	876	877	878	879	880	881	882	883	884	885	886	887	888	889	890	891	892	893	894	895	896	897	898	899	900	901	902	903	904	905	906	907	908	909	910	911	912	913	914	915	916	917	918	919	920	921	922	923	924	925	926	927	928	929	930	931	932	933	934	935	936	937	938	939	940	941	942	943	944	945	946	947	948	949	950	951	952	953	954	955	956	957	958	959	960	961	962	963	964	965	966	967	968	969	970	971	972	973	974	975	976	977	978	979	980	981	982	983	984	985	986	987	988	989	990	991	992	993	994	995	996	997	998	999	9999

Table 2: Audio encoder ablation in the cross-sync setting.

Audio Encoder. We also investigate the impact of different audio encoders on the generated videos, as shown in Table 2. We see that Wav2vec2 Baevski et al. (2020) produces marginally higher video quality, as indicated by its lower FVD score. However, this comes at the expense of lip synchronization, as reflected in its lower LipScore. With WavLM Chen et al. (2022), we achieve a LipScore comparable to HuBERT Hsu et al. (2021), but at the cost of worse video quality. In contrast, HuBERT maintains a strong LipScore and achieves the lowest LipLeak, indicating effective mitigation of expression leakage. Therefore, we select HuBERT as our default audio encoder.

451	452	453	454	455	456	457	458	459	460	461	462	463	464	465	466	467	468	469	470	471	472	473	474	475	476	477	478	479	480	481	482	483	484	485	486	487	488	489	490	491	492	493	494	495	496	497	498	499	500	501	502	503	504	505	506	507	508	509	510	511	512	513	514	515	516	517	518	519	520	521	522	523	524	525	526	527	528	529	530	531	532	533	534	535	536	537	538	539	540	541	542	543	544	545	546	547	548	549	550	551	552	553	554	555	556	557	558	559	560	561	562	563	564	565	566	567	568	569	570	571	572	573	574	575	576	577	578	579	580	581	582	583	584	585	586	587	588	589	590	591	592	593	594	595	596	597	598	599	600	601	602	603	604	605	606	607	608	609	610	611	612	613	614	615	616	617	618	619	620	621	622	623	624	625	626	627	628	629	630	631	632	633	634	635	636	637	638	639	640	641	642	643	644	645	646	647	648	649	650	651	652	653	654	655	656	657	658	659	660	661	662	663	664	665	666	667	668	669	670	671	672	673	674	675	676	677	678	679	680	681	682	683	684	685	686	687	688	689	690	691	692	693	694	695	696	697	698	699	700	701	702	703	704	705	706	707	708	709	710	711	712	713	714	715	716	717	718	719	720	721	722	723	724	725	726	727	728	729	730	731	732	733	734	735	736	737	738	739	740	741	742	743	744	745	746	747	748	749	750	751	752	753	754	755	756	757	758	759	760	761	762	763	764	765	766	767	768	769	770	771	772	773	774	775	776	777	778	779	780	781	782	783	784	785	786	787	788	789	790	791	792	793	794	795	796	797	798	799	800	801	802	803	804	805	806	807	808	809	810	811	812	813	814	815	816	817	818	819	820	821	822	823	824	825	826	827	828	829	830	831	832	833	834	835	836	837	838	839	840	841	842	843	844	845	846	847	848	849	850	851	852	853	854	855	856	857	858	859	860	861	862	863	864	865	866	867	868	869	870	871	872	873	874	875	876	877	878	879	880	881	882	883	884	885	886	887	888	889	890	891	892	893	894	895	896	897	898	899	900	901	902	903	904	905	906	907	908	909	910	911	912	913	914	915	916	917	918	919	920	921	922	923	924	925	926	927	928	929	930	931	932	933	934	935	936	937	938	939	940	941	942	943	944	945	946	947	948	949	950	951	952	953	954	955	956	957	958	959	960	961	962	963	964	965	966	967	968	969	970	971	972	973	974	975	976	977	978	979	980	981	982	983	984	985	986	987	988	989	990	991	992	993	994	995	996	997	998	999	9999

451	452	453	454	455	456	457	458	459	460	461	462	463	464	465	466	467	468	469	470	471	472	473	474	475	476	477	478	479	480	481	482	483	484	485	486	487	488	489	490	491	492	493	494	495	496	497	498	499	500	501	502	503	504	505	506	507	508	509	510	511	512	513	514	515	516	517	518	519	520	521	522	523	524	525	526	527	528	529	530	531	532	533	534	535	536	537	538	539	540	541	542	543	544	545	546	547	548	549	550	551	552	553	554	555	556	557	558	559	560	561	562	563	564	565	566	567	568	569	570	571	572	573	574	575	576	577	578	579	580	581	582	583	584	585	586	587	588	589	590	591	592	593	594	595	596	597	598	599	600	601	602	603	604	605	606	607	608	609	610	611	612	613	614	615	616	617	618	619	620	621	622	623	624	625	626	627	628	629	630	631	632	633	634	635	636	637	638	639	640	641	642	643	644	645	646	647	648	649	650	651	652	653	654	655	656	657	658	659	660	661	662	663	664	665	666	667	668	669	670	671	672	673	674	675	676	677	678	679	680	681	682	683	684	685	686	687	688	689	690	691	692	693	694	695	696	697	698	699	700	70

486 REFERENCES
487

488 Alexei Baevski, Yuhao Zhou, Abdelrahman Mohamed, and Michael Auli. wav2vec
489 2.0: A framework for self-supervised learning of speech representations. In Hugo
490 Larochelle, Marc'Aurelio Ranzato, Raia Hadsell, Maria-Florina Balcan, and Hsuan-Tien
491 Lin (eds.), *Advances in Neural Information Processing Systems 33: Annual Conference
492 on Neural Information Processing Systems 2020, NeurIPS 2020, December 6-12, 2020,
493 virtual*, 2020. URL <https://proceedings.neurips.cc/paper/2020/hash/92d1e1eb1cd6f9fba3227870bb6d7f07-Abstract.html>.

494

495 Antoni Bigata, Michał Stypułkowski, Rodrigo Mira, Stella Bounareli, Konstantinos Vougioukas,
496 Zoe Landgraf, Nikita Drobyshev, Maciej Zieba, Stavros Petridis, and Maja Pantic. Keyface:
497 Expressive audio-driven facial animation for long sequences via keyframe interpolation, 2025.
498 URL <https://arxiv.org/abs/2503.01715>.

499

500 Dan Bigioi, Shubhajit Basak, Michal Stypulkowski, Maciej Zieba, Hugh Jordan, Rachel McDonnell,
501 and Peter Corcoran. Speech driven video editing via an audio-conditioned diffusion model. *Image
502 Vis. Comput.*, 142:104911, 2024. doi: 10.1016/J.IMAVIS.2024.104911. URL <https://doi.org/10.1016/j.imavis.2024.104911>.

503

504 Andreas Blattmann, Tim Dockhorn, Sumith Kulal, Daniel Mendelevitch, Maciej Kilian, Dominik
505 Lorenz, Yam Levi, Zion English, Vikram Voleti, Adam Letts, Varun Jampani, and Robin Rom-
506 bach. Stable video diffusion: Scaling latent video diffusion models to large datasets, 2023. URL
507 <https://arxiv.org/abs/2311.15127>.

508

509 Adrian Bulat and Georgios Tzimiropoulos. How far are we from solving the 2d & 3d face alignment
510 problem? (and a dataset of 230, 000 3d facial landmarks). In *IEEE International Conference on
511 Computer Vision, ICCV 2017, Venice, Italy, October 22-29, 2017*, pp. 1021–1030. IEEE Com-
512 puter Society, 2017. doi: 10.1109/ICCV.2017.116. URL <https://doi.org/10.1109/ICCV.2017.116>.

513

514 Chaofeng Chen and Jiadi Mo. IQA-PyTorch: Pytorch toolbox for image quality assessment. [On-
515 line]. Available: <https://github.com/chaofengc/IQA-PyTorch>, 2022.

516

517 Chaofeng Chen, Jiadi Mo, Jingwen Hou, Haoning Wu, Liang Liao, Wenxiu Sun, Qiong Yan, and
518 Weisi Lin. TOPIQ: A top-down approach from semantics to distortions for image quality assess-
519 ment. *IEEE Trans. Image Process.*, 33:2404–2418, 2024a. doi: 10.1109/TIP.2024.3378466. URL
520 <https://doi.org/10.1109/TIP.2024.3378466>.

521

522 Lele Chen, Guofeng Cui, Celong Liu, Zhong Li, Ziyi Kou, Yi Xu, and Chenliang Xu. Talking-head
523 generation with rhythmic head motion. In *European Conference on Computer Vision*, pp. 35–51.
524 Springer, 2020.

525

526 Sanyuan Chen, Chengyi Wang, Zhengyang Chen, Yu Wu, Shujie Liu, Zhuo Chen, Jinyu Li, Naoyuki
527 Kanda, Takuya Yoshioka, Xiong Xiao, Jian Wu, Long Zhou, Shuo Ren, Yanmin Qian, Yao Qian,
528 Jian Wu, Michael Zeng, Xiangzhan Yu, and Furu Wei. Wavlm: Large-scale self-supervised pre-
529 training for full stack speech processing. *IEEE J. Sel. Top. Signal Process.*, 16(6):1505–1518,
530 2022. doi: 10.1109/JSTSP.2022.3188113. URL <https://doi.org/10.1109/JSTSP.2022.3188113>.

531

532 Zhiyuan Chen, Jiajiong Cao, Zhiquan Chen, Yuming Li, and Chenguang Ma. Echomimic: Lifelike
533 audio-driven portrait animations through editable landmark conditions, 2024b. URL <https://arxiv.org/abs/2407.08136>.

534

535 Kun Cheng, Xiaodong Cun, Yong Zhang, Menghan Xia, Fei Yin, Mingrui Zhu, Xuan Wang, Jue
536 Wang, and Nannan Wang. Videoretalking: Audio-based lip synchronization for talking head video
537 editing in the wild. In Soon Ki Jung, Jehee Lee, and Adam W. Bargteil (eds.), *SIGGRAPH Asia
538 2022 Conference Papers, SA 2022, Daegu, Republic of Korea, December 6-9, 2022*, pp. 30:1–
539 30:9. ACM, 2022. doi: 10.1145/3550469.3555399. URL <https://doi.org/10.1145/3550469.3555399>.

540 Wei-Lin Chiang, Lianmin Zheng, Ying Sheng, Anastasios Nikolas Angelopoulos, Tianle Li,
 541 Dacheng Li, Hao Zhang, Banghua Zhu, Michael Jordan, Joseph E. Gonzalez, and Ion Stoica.
 542 Chatbot arena: An open platform for evaluating llms by human preference, 2024.
 543

544 Joon Son Chung and Andrew Zisserman. Out of time: Automated lip sync in the wild. In
 545 Chu-Song Chen, Jiwen Lu, and Kai-Kuang Ma (eds.), *Computer Vision - ACCV 2016 Work-
 546 shops - ACCV 2016 International Workshops, Taipei, Taiwan, November 20-24, 2016, Revised
 547 Selected Papers, Part II*, volume 10117 of *Lecture Notes in Computer Science*, pp. 251–263.
 548 Springer, 2016. doi: 10.1007/978-3-319-54427-4_19. URL https://doi.org/10.1007/978-3-319-54427-4_19.
 549

550 Joon Son Chung, Amir Jamaludin, and Andrew Zisserman. You said that? *arXiv preprint
 551 arXiv:1705.02966*, 2017.

552 Prafulla Dhariwal and Alexander Quinn Nichol. Diffusion models beat gans on image synthesis. In
 553 Marc'Aurelio Ranzato, Alina Beygelzimer, Yann N. Dauphin, Percy Liang, and Jennifer Wortman
 554 Vaughan (eds.), *Advances in Neural Information Processing Systems 34: Annual Conference on
 555 Neural Information Processing Systems 2021, NeurIPS 2021, December 6-14, 2021, virtual*, pp.
 556 8780–8794, 2021. URL <https://proceedings.neurips.cc/paper/2021/hash/49ad23d1ec9fa4bd8d77d02681df5cfa-Abstract.html>.
 557

558 Arpad E. Elo. *The Rating of Chessplayers, Past and Present*. Arco Pub., New
 559 York, 1978. ISBN 0668047216 9780668047210. URL <http://www.amazon.com/Rating-Chess-Players-Past-Present/dp/0668047216>.
 560

561 Ian J. Goodfellow, Jean Pouget-Abadie, Mehdi Mirza, Bing Xu, David Warde-Farley, Sherjil
 562 Ozair, Aaron C. Courville, and Yoshua Bengio. Generative adversarial networks. *Commun.
 563 ACM*, 63(11):139–144, 2020. doi: 10.1145/3422622. URL <https://doi.org/10.1145/3422622>.
 564

565 Jiazh Guan, Zhanwang Zhang, Hang Zhou, Tianshu Hu, Kaisiyuan Wang, Dongliang He, Haocheng
 566 Feng, Jingtuo Liu, Errui Ding, Ziwei Liu, et al. Stylesync: High-fidelity generalized and personal-
 567 ized lip sync in style-based generator. In *Proceedings of the IEEE/CVF Conference on Computer
 568 Vision and Pattern Recognition*, pp. 1505–1515, 2023.
 569

570 Jonathan Ho. Classifier-free diffusion guidance. *ArXiv*, abs/2207.12598, 2022. URL <https://api.semanticscholar.org/CorpusID:249145348>.
 571

572 Jonathan Ho, Ajay Jain, and Pieter Abbeel. Denoising diffusion probabilistic models. In
 573 Hugo Larochelle, Marc'Aurelio Ranzato, Raia Hadsell, Maria-Florina Balcan, and Hsuan-
 574 Tien Lin (eds.), *Advances in Neural Information Processing Systems 33: Annual Con-
 575 ference on Neural Information Processing Systems 2020, NeurIPS 2020, December 6-12,
 576 2020, virtual*, 2020. URL <https://proceedings.neurips.cc/paper/2020/hash/4c5bcfec8584af0d967f1ab10179ca4b-Abstract.html>.
 577

578 Jonathan Ho, Chitwan Saharia, William Chan, David J. Fleet, Mohammad Norouzi, and Tim Salis-
 579 mans. Cascaded diffusion models for high fidelity image generation. *J. Mach. Learn. Res.*, 23:
 580 47:1–47:33, 2022. URL <https://jmlr.org/papers/v23/21-0635.html>.
 581

582 Wei-Ning Hsu, Benjamin Bolte, Yao-Hung Hubert Tsai, Kushal Lakhota, Ruslan Salakhutdinov,
 583 and Abdelrahman Mohamed. Hubert: Self-supervised speech representation learning by masked
 584 prediction of hidden units. *IEEE ACM Trans. Audio Speech Lang. Process.*, 29:3451–3460, 2021.
 585 doi: 10.1109/TASLP.2021.3122291. URL <https://doi.org/10.1109/TASLP.2021.3122291>.
 586

587 Li Hu. Animate anyone: Consistent and controllable image-to-video synthesis for character anima-
 588 tion. In *IEEE/CVF Conference on Computer Vision and Pattern Recognition, CVPR 2024, Seattle,
 589 WA, USA, June 16-22, 2024*, pp. 8153–8163. IEEE, 2024. doi: 10.1109/CVPR52733.2024.00779.
 590 URL <https://doi.org/10.1109/CVPR52733.2024.00779>.
 591

592 Sadeep Jayasumana, Srikumar Ramalingam, Andreas Veit, Daniel Glasner, Ayan Chakrabarti, and
 593 Sanjiv Kumar. Rethinking FID: towards a better evaluation metric for image generation. In

594 *IEEE/CVF Conference on Computer Vision and Pattern Recognition, CVPR 2024, Seattle, WA,*
 595 *USA, June 16-22, 2024, pp. 9307–9315. IEEE, 2024. doi: 10.1109/CVPR52733.2024.00889.*
 596 URL <https://doi.org/10.1109/CVPR52733.2024.00889>.

597 R Kannan, Palamakula Jahnavi, and M Megha. Driver drowsiness detection and alert system. In
 598 *2023 IEEE International Conference on Integrated Circuits and Communication Systems (ICI-*
 599 *CACS)*, pp. 1–5, 2023. doi: [10.1109/ICICACS57338.2023.10100316](https://doi.org/10.1109/ICICACS57338.2023.10100316).

601 Tero Karras, Miika Aittala, Timo Aila, and Samuli Laine. Elucidating the design
 602 space of diffusion-based generative models. In Sanmi Koyejo, S. Mohamed, A. Agar-
 603 wal, Danielle Belgrave, K. Cho, and A. Oh (eds.), *Advances in Neural Informa-*
 604 *tion Processing Systems 35: Annual Conference on Neural Information Processing Sys-*
 605 *tems 2022, NeurIPS 2022, New Orleans, LA, USA, November 28 - December 9,*
 606 *2022, 2022*. URL http://papers.nips.cc/paper_files/paper/2022/hash/a98846e9d9cc01cfb87eb694d946ce6b-Abstract-Conference.html.

607 Taekyung Ki and Dongchan Min. Stylelipsync: Style-based personalized lip-sync video generation.
 608 In *IEEE/CVF International Conference on Computer Vision, ICCV 2023, Paris, France, October*
 609 *1-6, 2023, pp. 22784–22793. IEEE, 2023. doi: 10.1109/ICCV51070.2023.02088. URL https:*
 610 */doi.org/10.1109/ICCV51070.2023.02088*.

611 Chunyu Li, Chao Zhang, Weikai Xu, Jinghui Xie, Weiguo Feng, Bingyue Peng, and Weiwei Xing.
 612 Latentsync: Audio conditioned latent diffusion models for lip sync. *CoRR*, abs/2412.09262, 2024.
 613 doi: [10.48550/ARXIV.2412.09262](https://arxiv.org/abs/2412.09262). URL <https://doi.org/10.48550/arXiv.2412.09262>.

614 Junhua Liao, Haihan Duan, Kanghui Feng, Wanbing Zhao, Yanbing Yang, and Liangyin Chen. A
 615 light weight model for active speaker detection. In *Proceedings of the IEEE/CVF Conference on*
 616 *Computer Vision and Pattern Recognition (CVPR)*, pp. 22932–22941, June 2023.

617 Tao Liu, Chenpeng Du, Shuai Fan, Feilong Chen, and Kai Yu. Diffdub: Person-generic visual
 618 dubbing using inpainting renderer with diffusion auto-encoder. In *IEEE International Conference*
 619 *on Acoustics, Speech and Signal Processing, ICASSP 2024, Seoul, Republic of Korea, April 14-19,*
 620 *2024, pp. 3630–3634. IEEE, 2024. doi: 10.1109/ICASSP48485.2024.10446049. URL https:*
 621 */doi.org/10.1109/ICASSP48485.2024.10446049*.

622 Andreas Lugmayr, Martin Danelljan, Andrés Romero, Fisher Yu, Radu Timofte, and Luc Van Gool.
 623 Repaint: Inpainting using denoising diffusion probabilistic models. In *IEEE/CVF Conference*
 624 *on Computer Vision and Pattern Recognition, CVPR 2022, New Orleans, LA, USA, June 18-24,*
 625 *2022, pp. 11451–11461. IEEE, 2022. doi: 10.1109/CVPR52688.2022.01117. URL https:*
 626 */doi.org/10.1109/CVPR52688.2022.01117*.

627 Urwa Muaz, Wondong Jang, Rohun Tripathi, Santhosh Mani, Wenbin Ouyang, Ravi Teja Gadde,
 628 Baris Gecer, Sergio Elizondo, Reza Madad, and Naveen Nair. SIDGAN: high-resolution dubbed
 629 video generation via shift-invariant learning. In *IEEE/CVF International Conference on Com-*
 630 *puter Vision, ICCV 2023, Paris, France, October 1-6, 2023, pp. 7799–7808. IEEE, 2023.*
 631 doi: [10.1109/ICCV51070.2023.00720](https://doi.org/10.1109/ICCV51070.2023.00720). URL <https://doi.org/10.1109/ICCV51070.2023.00720>.

632 Soumik Mukhopadhyay, Saksham Suri, Ravi Teja Gadde, and Abhinav Shrivastava. Diff2lip: Audio
 633 conditioned diffusion models for lip-synchronization. In *IEEE/CVF Winter Conference on Appli-*
 634 *cations of Computer Vision, WACV 2024, Waikoloa, HI, USA, January 3-8, 2024, pp. 5280–5290.*
 635 IEEE, 2024. doi: [10.1109/WACV57701.2024.00521](https://doi.org/10.1109/WACV57701.2024.00521). URL <https://doi.org/10.1109/WACV57701.2024.00521>.

636 Se Jin Park, Minsu Kim, Joanna Hong, Jeongsoo Choi, and Yong Man Ro. SyncTalkface: Talking
 637 face generation with precise lip-syncing via audio-lip memory. In *Thirty-Sixth AAAI Conference*
 638 *on Artificial Intelligence, AAAI 2022, Thirty-Fourth Conference on Innovative Applications of*
 639 *Artificial Intelligence, IAAI 2022, The Twelveth Symposium on Educational Advances in Artificial*
 640 *Intelligence, EAAI 2022 Virtual Event, February 22 - March 1, 2022, pp. 2062–2070. AAAI*
 641 *Press, 2022. doi: 10.1609/AAAI.V36I2.20102. URL https://doi.org/10.1609/aaai.v36i2.20102*.

648 J.L. Pech-Pacheco, G. Cristobal, J. Chamorro-Martinez, and J. Fernandez-Valdivia. Diatom aut-
 649 ofocusing in brightfield microscopy: a comparative study. In *Proceedings 15th International*
 650 *Conference on Pattern Recognition. ICPR-2000*, volume 3, pp. 314–317 vol.3, 2000. doi:
 651 10.1109/ICPR.2000.903548.

652 Ziqiao Peng, Jiwen Liu, Haoxian Zhang, Xiaoqiang Liu, Songlin Tang, Pengfei Wan, Di Zhang,
 653 Hongyan Liu, and Jun He. Omnisync: Towards universal lip synchronization via diffusion trans-
 654 formers. *CoRR*, abs/2505.21448, 2025. doi: 10.48550/ARXIV.2505.21448. URL <https://doi.org/10.48550/arXiv.2505.21448>.

655 KR Prajwal, Rudrabha Mukhopadhyay, Vinay P Namboodiri, and CV Jawahar. A lip sync expert is
 656 all you need for speech to lip generation in the wild. In *Proceedings of the 28th ACM International*
 657 *Conference on Multimedia*, pp. 484–492, 2020.

658 Weize Quan, Jiaxi Chen, Yanli Liu, Dong-Ming Yan, and Peter Wonka. Deep learning-based image
 659 and video inpainting: A survey. *Int. J. Comput. Vis.*, 132(7):2367–2400, 2024. doi: 10.1007/
 660 S11263-023-01977-6. URL <https://doi.org/10.1007/s11263-023-01977-6>.

661 Alec Radford, Jong Wook Kim, Tao Xu, Greg Brockman, Christine McLeavey, and Ilya Sutskever.
 662 Robust speech recognition via large-scale weak supervision. In *International conference on ma-*
 663 *chine learning*, pp. 28492–28518. PMLR, 2023.

664 Nikhila Ravi, Valentin Gabeur, Yuan-Ting Hu, Ronghang Hu, Chaitanya Ryali, Tengyu Ma, Haitham
 665 Khedr, Roman Rädle, Chloé Rolland, Laura Gustafson, Eric Mintun, Junting Pan, Kalyan Va-
 666 sudev Alwala, Nicolas Carion, Chao-Yuan Wu, Ross B. Girshick, Piotr Dollár, and Christoph
 667 Feichtenhofer. SAM 2: Segment anything in images and videos. *CoRR*, abs/2408.00714, 2024.
 668 doi: 10.48550/ARXIV.2408.00714. URL [https://doi.org/10.48550/arXiv.2408.](https://doi.org/10.48550/arXiv.2408.00714)
 669 00714.

670 Robin Rombach, Andreas Blattmann, Dominik Lorenz, Patrick Esser, and Björn Ommer. High-
 671 resolution image synthesis with latent diffusion models. In *IEEE/CVF Conference on Com-*
 672 *puter Vision and Pattern Recognition, CVPR 2022, New Orleans, LA, USA, June 18-24, 2022*,
 673 pp. 10674–10685. IEEE, 2022. doi: 10.1109/CVPR52688.2022.01042. URL <https://doi.org/10.1109/CVPR52688.2022.01042>.

674 Chitwan Saharia, William Chan, Huiwen Chang, Chris A. Lee, Jonathan Ho, Tim Salimans, David J.
 675 Fleet, and Mohammad Norouzi. Palette: Image-to-image diffusion models. In Munkhtsetseg
 676 Nandigjav, Niloy J. Mitra, and Aaron Hertzmann (eds.), *SIGGRAPH '22: Special Interest Group*
 677 *on Computer Graphics and Interactive Techniques Conference, Vancouver, BC, Canada, August*
 678 *7 - 11, 2022*, pp. 15:1–15:10. ACM, 2022. doi: 10.1145/3528233.3530757. URL <https://doi.org/10.1145/3528233.3530757>.

679 Axel Sauer, Dominik Lorenz, Andreas Blattmann, and Robin Rombach. Adversarial diffusion dis-
 680 tillation. In Ales Leonardis, Elisa Ricci, Stefan Roth, Olga Russakovsky, Torsten Sattler, and
 681 Gü̈l Varol (eds.), *Computer Vision - ECCV 2024 - 18th European Conference, Milan, Italy,*
 682 *September 29-October 4, 2024, Proceedings, Part LXXXVI*, volume 15144 of *Lecture Notes in*
 683 *Computer Science*, pp. 87–103. Springer, 2024. doi: 10.1007/978-3-031-73016-0_6. URL
 684 https://doi.org/10.1007/978-3-031-73016-0_6.

685 Shuai Shen, Wenliang Zhao, Zibin Meng, Wanhua Li, Zheng Zhu, Jie Zhou, and Jiwen Lu. DiffTalk:
 686 Crafting diffusion models for generalized audio-driven portraits animation. In *IEEE/CVF Con-*
 687 *ference on Computer Vision and Pattern Recognition, CVPR 2023, Vancouver, BC, Canada,*
 688 *June 17-24, 2023*, pp. 1982–1991. IEEE, 2023. doi: 10.1109/CVPR52729.2023.00197. URL
 689 <https://doi.org/10.1109/CVPR52729.2023.00197>.

690 Yang Song, Prafulla Dharwal, Mark Chen, and Ilya Sutskever. Consistency models. *CoRR*,
 691 abs/2303.01469, 2023. doi: 10.48550/ARXIV.2303.01469. URL <https://doi.org/10.48550/arXiv.2303.01469>.

692 Michal Stypulkowski, Konstantinos Vougioukas, Sen He, Maciej Zieba, Stavros Petridis, and Maja
 693 Pantic. Diffused heads: Diffusion models beat gans on talking-face generation. In *IEEE/CVF*
 694 *Winter Conference on Applications of Computer Vision, WACV 2024, Waikoloa, HI, USA, January*

702 3-8, 2024, pp. 5089–5098. IEEE, 2024. doi: 10.1109/WACV57701.2024.00502. URL <https://doi.org/10.1109/WACV57701.2024.00502>.

703

704

705 Shaolin Su, Qingsen Yan, Yu Zhu, Cheng Zhang, Xin Ge, Jinqiu Sun, and Yanning Zhang. Blindly
706 assess image quality in the wild guided by a self-adaptive hyper network. In *IEEE/CVF Conference
707 on Computer Vision and Pattern Recognition (CVPR)*, June 2020.

708

709 Thomas Unterthiner, Sjoerd van Steenkiste, Karol Kurach, Raphael Marinier, Marcin Michalski,
710 and Sylvain Gelly. Towards accurate generative models of video: A new metric and challenges,
711 2019. URL <https://arxiv.org/abs/1812.01717>.

712

713 Konstantinos Vougioukas, Stavros Petridis, and Maja Pantic. Realistic speech-driven facial anima-
714 tion with gans. *International Journal of Computer Vision*, pp. 1–16, 2019.

715

716 Jiadong Wang, Xinyuan Qian, Malu Zhang, Robby T. Tan, and Haizhou Li. Seeing what you said:
717 Talking face generation guided by a lip reading expert. In *IEEE/CVF Conference on Computer
718 Vision and Pattern Recognition, CVPR 2023, Vancouver, BC, Canada, June 17-24, 2023*, pp.
719 14653–14662. IEEE, 2023a. doi: 10.1109/CVPR52729.2023.01408. URL <https://doi.org/10.1109/CVPR52729.2023.01408>.

720

721 Jiayu Wang, Kang Zhao, Shiwei Zhang, Yingya Zhang, Yujun Shen, Deli Zhao, and Jingren
722 Zhou. Lipformer: High-fidelity and generalizable talking face generation with A pre-learned
723 facial codebook. In *IEEE/CVF Conference on Computer Vision and Pattern Recognition,
724 CVPR 2023, Vancouver, BC, Canada, June 17-24, 2023*, pp. 13844–13853. IEEE, 2023b.
725 doi: 10.1109/CVPR52729.2023.01330. URL <https://doi.org/10.1109/CVPR52729.2023.01330>.

726

727 Huawei Wei, Zejun Yang, and Zhisheng Wang. Aniportrait: Audio-driven synthesis of photorealistic
728 portrait animation, 2024. URL <https://arxiv.org/abs/2403.17694>.

729

730 Mingwang Xu, Hui Li, Qingkun Su, Hanlin Shang, Liwei Zhang, Ce Liu, Jingdong Wang, Yao Yao,
731 and Siyu Zhu. Hallo: Hierarchical audio-driven visual synthesis for portrait image animation,
732 2024a. URL <https://arxiv.org/abs/2406.08801>.

733

734 Sicheng Xu, Guojun Chen, Yu-Xiao Guo, Jiaolong Yang, Chong Li, Zhenyu Zang, Yizhong Zhang,
735 Xin Tong, and Baining Guo. Vasa-1: Lifelike audio-driven talking faces generated in real time.
arXiv preprint arXiv:2404.10667, 2024b.

736

737 Dogucan Yaman, Fevziye Irem Eyiokur, Leonard Bärmann, Hazim Kemal Ekenel, and Alexan-
738 der Waibel. Audio-driven talking face generation with stabilized synchronization loss. In
739 Ales Leonardis, Elisa Ricci, Stefan Roth, Olga Russakovsky, Torsten Sattler, and Gü̈l Varol
740 (eds.), *Computer Vision - ECCV 2024 - 18th European Conference, Milan, Italy, September
741 29-October 4, 2024, Proceedings, Part XIX*, volume 15077 of *Lecture Notes in Computer
742 Science*, pp. 417–435. Springer, 2024. doi: 10.1007/978-3-031-72655-2_24. URL https://doi.org/10.1007/978-3-031-72655-2_24.

743

744 Jianhui Yu, Hao Zhu, Liming Jiang, Chen Change Loy, Weidong Cai, and Wayne Wu. CelebV-Text:
745 A large-scale facial text-video dataset. In *CVPR*, 2023.

746

747 Runyi Yu, Tianyu He, Ailing Zhang, Yuchi Wang, Junliang Guo, Xu Tan, Chang Liu, Jie Chen,
748 and Jiang Bian. Make your actor talk: Generalizable and high-fidelity lip sync with motion and
749 appearance disentanglement. *CoRR*, abs/2406.08096, 2024. doi: 10.48550/ARXIV.2406.08096.
750 URL <https://doi.org/10.48550/arXiv.2406.08096>.

751

752 Fangneng Zhan, Yingchen Yu, Rongliang Wu, Jiahui Zhang, Shijian Lu, Lingjie Liu, Adam Ko-
753 rtylewski, Christian Theobalt, and Eric Xing. Multimodal image synthesis and editing: A survey
754 and taxonomy. *IEEE Transactions on Pattern Analysis and Machine Intelligence*, 2023.

755

756 Chenxu Zhang, Chao Wang, Jianfeng Zhang, Hongyi Xu, Guoxian Song, You Xie, Linjie Luo,
757 Yapeng Tian, Xiaohu Guo, and Jiashi Feng. Dream-talk: diffusion-based realistic emotional
758 audio-driven method for single image talking face generation. *arXiv preprint arXiv:2312.13578*,
759 2023a.

756 David Junhao Zhang, Jay Zhangjie Wu, Jia-Wei Liu, Rui Zhao, Lingmin Ran, Yuchao Gu, Difei
 757 Gao, and Mike Zheng Shou. Show-1: Marrying pixel and latent diffusion models for text-to-
 758 video generation. *CoRR*, abs/2309.15818, 2023b. doi: 10.48550/ARXIV.2309.15818. URL
 759 <https://doi.org/10.48550/arXiv.2309.15818>.

760 Wenxuan Zhang, Xiaodong Cun, Xuan Wang, Yong Zhang, Xi Shen, Yu Guo, Ying Shan, and Fei
 761 Wang. Sadtalker: Learning realistic 3d motion coefficients for stylized audio-driven single image
 762 talking face animation. In *IEEE/CVF Conference on Computer Vision and Pattern Recognition*,
 763 *CVPR 2023, Vancouver, BC, Canada, June 17-24, 2023*, pp. 8652–8661. IEEE, 2023c. doi: 10.
 764 1109/CVPR52729.2023.00836. URL <https://doi.org/10.1109/CVPR52729.2023.00836>.

765 Yue Zhang, Minhao Liu, Zhaokang Chen, Bin Wu, Yubin Zeng, Chao Zhan, Yingjie He, Junxin
 766 Huang, and Wenjiang Zhou. MuseTalk: Real-Time High Quality Lip Synchronization with
 767 Latent Space Inpainting, October 2024. URL <http://arxiv.org/abs/2410.10122>.
 768 arXiv:2410.10122 [cs].

769 Zhimeng Zhang, Lincheng Li, Yu Ding, and Changjie Fan. Flow-guided one-shot talking face gen-
 770 eration with a high-resolution audio-visual dataset. In *2021 IEEE/CVF Conference on Computer*
 771 *Vision and Pattern Recognition (CVPR)*, pp. 3660–3669, 2021. doi: 10.1109/CVPR46437.2021.
 772 00366.

773 Zhimeng Zhang, Zhipeng Hu, Wenjin Deng, Changjie Fan, Tangjie Lv, and Yu Ding. Dinet: Defor-
 774 mation inpainting network for realistic face visually dubbing on high resolution video. In Brian
 775 Williams, Yiling Chen, and Jennifer Neville (eds.), *Thirty-Seventh AAAI Conference on Artificial*
 776 *Intelligence, AAAI 2023, Thirty-Fifth Conference on Innovative Applications of Artificial Intelli-
 777 gence, IAAI 2023, Thirteenth Symposium on Educational Advances in Artificial Intelligence, EAAI*
 778 *2023, Washington, DC, USA, February 7-14, 2023*, pp. 3543–3551. AAAI Press, 2023d. doi:
 779 10.1609/AAAI.V37I3.25464. URL <https://doi.org/10.1609/aaai.v37i3.25464>.

780 Rui Zhen, Wenchao Song, Qiang He, Juan Cao, Lei Shi, and Jia Luo. Human-computer interaction
 781 system: A survey of talking-head generation. *Electronics*, 12(1):218, 2023.

782 Weizhi Zhong, Chaowei Fang, Yinqi Cai, Pengxu Wei, Gangming Zhao, Liang Lin, and Guanbin Li.
 783 Identity-preserving talking face generation with landmark and appearance priors. In *Proceedings*
 784 *of the IEEE/CVF Conference on Computer Vision and Pattern Recognition (CVPR)*, pp. 9729–
 785 9738, June 2023.

786 Weizhi Zhong, Jichang Li, Yinqi Cai, Liang Lin, and Guanbin Li. Style-preserving lip sync via
 787 audio-aware style reference. *CoRR*, abs/2408.05412, 2024. doi: 10.48550/ARXIV.2408.05412.
 788 URL <https://doi.org/10.48550/arXiv.2408.05412>.

789 Hang Zhou, Yu Liu, Ziwei Liu, Ping Luo, and Xiaogang Wang. Talking face generation by ad-
 790 versarially disentangled audio-visual representation. In *Proceedings of the AAAI conference on*
 791 *artificial intelligence*, volume 33, pp. 9299–9306, 2019.

792 Hang Zhou, Yasheng Sun, Wayne Wu, Chen Change Loy, Xiaogang Wang, and Ziwei Liu. Pose-
 793 controllable talking face generation by implicitly modularized audio-visual representation. In
 794 *Proceedings of the IEEE/CVF conference on computer vision and pattern recognition*, pp. 4176–
 795 4186, 2021.

796 Hao Zhu, Wayne Wu, Wentao Zhu, Liming Jiang, Siwei Tang, Li Zhang, Ziwei Liu, and
 797 Chen Change Loy. CelebV-HQ: A large-scale video facial attributes dataset. In *ECCV*, 2022.

800

801

802

803

804

805

806

807

808

809

810
811 A DATASETS812 A.1 CURATION AND PREPROCESSING
813

814 When working with in-the-wild datasets such as CelebV-HQ Zhu et al. (2022) and CelebV-Text Yu
815 et al. (2023), we observed that a significant portion of the data is of suboptimal quality. Common
816 issues include visible hands, camera movement, editing artifacts, and occlusions. Additionally, some
817 samples exhibit lower resolution than advertised. Examples of these issues are illustrated in Figure 8.
818 During training, we found that such videos negatively impacted model performance because their
819 visual content correlates poorly with the corresponding audio. To address these challenges, we
820 developed a data curation pipeline comprising the following steps:

- 821 • Extract videos at 25 FPS and single-channel audio at 16 kHz.
822
- 823 • Discard low-quality videos based on HyperIQA Su et al. (2020) scores below 0.4. Each
824 video’s score is computed as the average of nine evaluations: selecting the first, middle,
825 and last frames, each evaluated on three random crops.
826
- 827 • Detect and segment scenes using PySceneDetect¹.
828
- 829 • Remove clips without active speakers using Light-ASD Liao et al. (2023) indicated by the
830 score below 0.75.
831

838 Figure 8: Examples of problematic videos in CelebV-HQ and CelebV-Text.
839840 A.2 DATA STATISTICS
841

843 Table 5 describes the training/evaluation data used in this paper, specifying the number of speakers,
844 videos, average video duration, and total duration for each dataset. Additionally, to illustrate the
845 impact of our data curation pipeline, we present Table 6, which details the statistics of the datasets
846 before curation. Overall, we discard roughly 75 % of the original videos. Please note that CelebV-
847 HQ and CelebV-Text videos were split into shorter chunks during pre-processing, hence the higher
848 video count in Table 5.
849

850 Dataset	# Speakers	# Videos	Duration	
			851 Avg. (sec.)	852 Total (hrs.)
853 HDTF	264	318	139.08	12
854 CelebV-HQ	3,668	12,000	4.00	13
855 CelebV-Text	9,109	75,307	6.38	130

856 Table 5: Data statistics after curation and pre-processing.
857858 B IMPLEMENTATION DETAILS
859

860 **Code** The code and model weights will be released upon acceptance.
861

862 ¹<https://github.com/Breakthrough/PySceneDetect>
863

Dataset	# Videos	Duration	
		Avg. (sec.)	Total (hrs.)
HDTF	318	139.08	12
CelebV-HQ	35,666	6.86	68
CelebV-Text	70,000	14.35	279

Table 6: Data statistics before curation.

Hyperparameters & Training Configuration We summarize all the hyperparameters of our pipeline in Table 7. The weights of the U-Net and VAE are initialized from SVD Blattmann et al. (2023). The interpolation model undergoes more training steps because its task differs more significantly from the original task of SVD. The final hyperparameters were selected through extensive experimentation to find the optimal trade-off between lip-synchronization accuracy (LipScore), visual quality (FVD), and expression leakage (LipLeak).

To optimize memory efficiency, we apply \mathcal{L}_{rgb} to a randomly selected frame from the sequence, which we found to be sufficient for maintaining perceptual quality.

Hyperparameter	Final Value	Range Tested
Keyframe seq. length (T)	14	Fixed
Keyframe spacing (S)	12	Fixed
Interpolation seq. length (S)	12	Fixed
Keyframe training steps	60,000	N/A
LipLeak ϵ	10^{-5}	Fixed
Interpolation training steps	120,000	N/A
Training batch size	32	{16, 32}
Optimizer	AdamW	Fixed
Learning rate	10^{-5}	{ 10^{-4} , 10^{-5} }
Warmup steps	1,000	{1,000, 2,000}
Inference steps	10	Fixed
GPU used	A100	N/A
Video frame rate	25	Fixed
Audio sample rate	16,000	Fixed
Resolution	512×512	Fixed
Pixel loss weighting (λ_2)	1	{0, 0.5, 1.0}
Audio cond. drop rate	20%	{10%, 20%, 30%}
Identity cond. drop rate	10%	{5%, 10%, 20%}

Table 7: Final model hyperparameters and the ranges tested during development. "Fixed" denotes values set by the model architecture or data standards, while "N/A" denotes values not typically tuned.

Evaluation The results presented in Table 1 were generated from a single run due to the computational cost of executing the full suite of methods.

Practical Deployment A limitation of our model is its inference speed, which is not yet real-time. Nevertheless, our two-stage approach is faster than other diffusion-based methods (e.g., DiffDub, Diff2Lip, LatentSync) and competitive with some GANs, as shown in Table 8. This advantage stems from our framework's support for batched inference, a feature absent in autoregressive models.

Future work could focus on acceleration by adapting techniques from recent literature. For example, Consistency Models Song et al. (2023) can enable single-step generation by learning to map any point on a diffusion trajectory back to the origin. Other promising approaches, such as adversarial distillation Sauer et al. (2024), can also reduce a trained diffusion model to a single-step generator while maintaining high output quality.

<i>Diffusion-based Methods</i>					
Model	VideoReTalking	DiffDub	Diff2Lip	LatentSync	KeySync
FPS	0.17	0.69	1.56	2.50	3.84
<i>GAN-based Methods</i>					
Model	IP_LAP	Wav2Lip	TalkLip		
FPS	4.31	16.66	92.00		

Table 8: Inference speed comparison in Frames Per Second (FPS). Higher is better.

C MASKING

C.1 MASK DEFINITION

To create the mask defined in Section 3.2, we first compute 68 facial landmarks in 2D Bulat & Tzimiropoulos (2017) and then follow the procedure in Algorithm 1.

Algorithm 1 Create mask from landmarks

```

Require:  $L \in \mathbb{R}^{T \times K \times 2}$  ▷ landmarks for  $T$  frames
1:  $(H, W)$  ▷ image height and width
2:  $n$  (nose index, default 28) ▷ binary masks
Ensure:  $M \in \{0, 1\}^{T \times H \times W}$  ▷ initialise masks
3:  $M \leftarrow \mathbf{0}_{T \times H \times W}$  ▷ landmarks of frame  $t$ 
4: for  $t \leftarrow 0$  to  $T - 1$  do ▷  $y$ -coord. of the nose
5:    $P \leftarrow L_t$  ▷ left-most landmark index
6:    $h_c \leftarrow P_{n,y}$  ▷ right-most landmark index
7:    $l \leftarrow \arg \min_k P_{k,x}$ 
8:    $r \leftarrow \arg \max_k P_{k,x}$ 
9:    $p_1 \leftarrow (P_{l,x}, h_c)$ 
10:   $p_2 \leftarrow (P_{l,x}, H)$ 
11:   $p_3 \leftarrow (P_{r,x}, H)$ 
12:   $p_4 \leftarrow (P_{r,x}, h_c)$ 
13:  FILLPOLYGON( $M_t, [p_1, p_2, p_3, p_4], 1$ ) ▷ fill polygon
14: return  $M$ 

```

C.2 ALTERNATIVE MASKING

In Figure 9, we illustrate the different masking strategies for the methods analysed in Section 5. We observe that while the masks of IP_LAP and Diff2Lip are closest to our own, their performance is affected by a tight facial crop applied before masking. This crop, which typically extends to the jawline, can leak the state of the mouth and excludes other speech-related areas such as the throat, which is reflected in their leakage scores in Table 1.

TalkLip masks the lower part of the image but fails to cover the cheek region, which contains important cues about the mouth’s state, resulting in a high LipLeak score. The mask shape used by DiffDub is similar to ours, but because it does not extend to the bottom of the frame, the model can infer the mouth shape from the mask’s position relative to the chin. Similarly, LatentSync uses a fixed mask and preprocesses the video so the mouth is always contained within it; however, this allows the model to infer mouth movements based on the position of the head rather than the audio content.



Figure 9: Illustration of the masking strategy of baseline methods

982 D LEAKAGE METRIC

984 D.1 MAR CALCULATION

986 We introduce LipLeak as part of our evaluation pipeline for measuring expression leakage. The first
 987 step in computing LipLeak is to calculate the Mouth Aspect Ratio (MAR) from facial landmarks, as
 988 illustrated in Figure 10. This ratio quantifies the vertical openness of the mouth relative to its width,
 989 increasing as the mouth opens wider. Because LipLeak is based on a ratio, it is a scale-invariant
 990 measure, allowing for consistent evaluation across different video resolutions and face sizes.

992 D.2 ALTERNATIVE METRIC

994 While LipLeak is a reliable metric, it requires running the model twice (once with speech audio and
 995 once with silent audio). To create a simpler metric, we propose LipLeak_{lite}, which only requires a
 996 single run with silent audio. LipLeak_{lite} measures the proportion of time the mouth is open when the
 997 audio is silent. We found that models opening their mouths during silent periods appear unnatural to
 998 users, making this a critical failure mode for real-world scenarios. To determine whether the mouth
 999 is open, we apply a threshold to the MAR; based on visual inspection, we selected a threshold of
 1000 0.25, as any MAR below this value consistently represents a closed mouth.

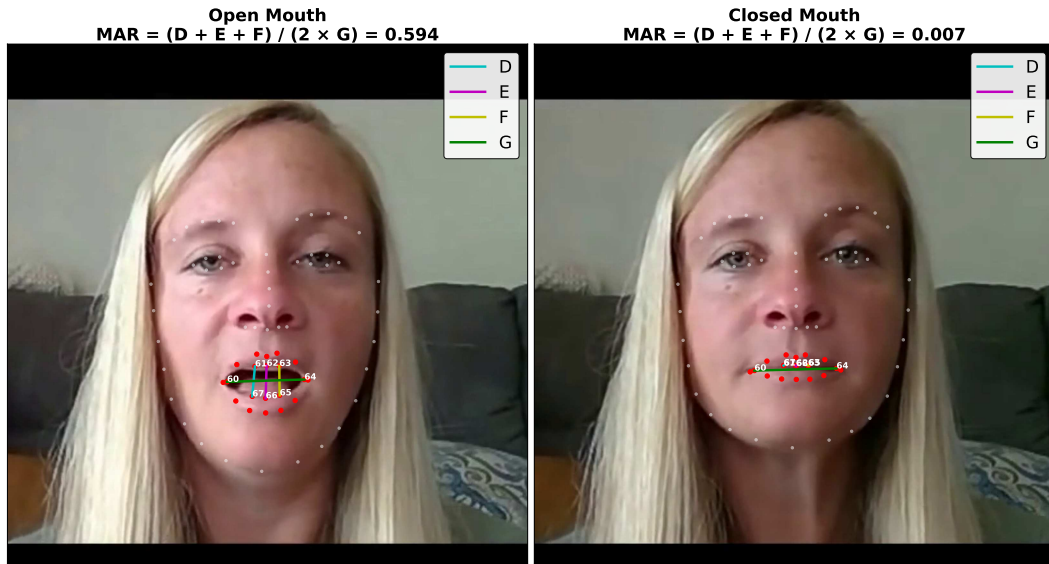


Figure 10: Mouth Aspect Ratio measurement example.

1022 To validate LipLeak_{lite}, we first assessed its sensitivity to this threshold. As shown in Figure 11,
 1023 LipLeak_{lite} decreases smoothly and predictably as the threshold increases. This stable behaviour is
 1024 essential for a reliable metric, as it prevents erratic jumps that could compromise quantitative eval-
 1025 uations. Finally, to ensure LipLeak_{lite} effectively captures the same underlying issue as LipLeak, we
 1026 computed the correlation between the two metrics in Figure 12. We observe a significant ($p < 0.05$)

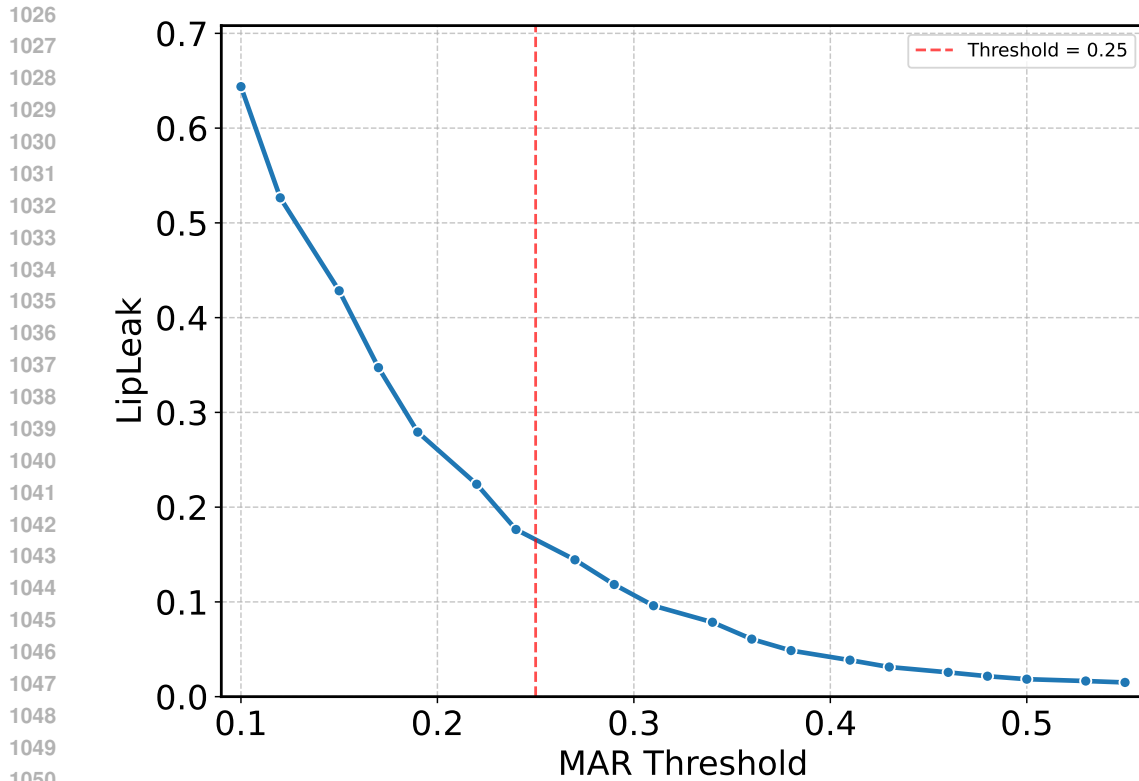


Figure 11: LipLeak as a function of the MAR threshold.

strong correlation between LipLeak_{lite} and LipLeak, confirming that LipLeak_{lite} is an efficient and reliable proxy for quantifying model leakage.

We note that a model could trivially achieve a low LipLeak score by producing minimal mouth motion for all inputs; however, such behavior would be heavily penalized by our primary sync metric, LipScore, which measures the positive correlation between audio and visual speech cues.

E OCCLUSION HANDLING

Handling occlusions via an external, state-of-the-art segmentation model is a deliberate design choice that provides significant flexibility. This modular approach allows us to benefit from rapid advancements in video segmentation without architectural changes or retraining. Any improvement in segmentation technology can be directly integrated, immediately boosting the system’s robustness. The trade-off is a dependency on this upstream component, as segmentation failures can propagate into the final result.

Figure 13 illustrates the application of our occlusion handling technique to several existing methods:

- **DiffDub Liu et al. (2024) and Diff2Lip Mukhopadhyay et al. (2024):** Our approach works out of the box, seamlessly handling occlusions without requiring modifications.
- **LatentSync Li et al. (2024):** Since this method employs a fixed mask, the model has never been exposed to variations in masking. As a result, it struggles to adapt to the new mask patterns introduced by our occlusion-handling technique, highlighting a key drawback of using a rigid masking approach.
- **IP LAP Zhong et al. (2023):** This model generates the mouth region separately through an audio-to-landmark module. Consequently, the occlusion mask has no direct effect, and the mouth is generated on top of the occlusion.

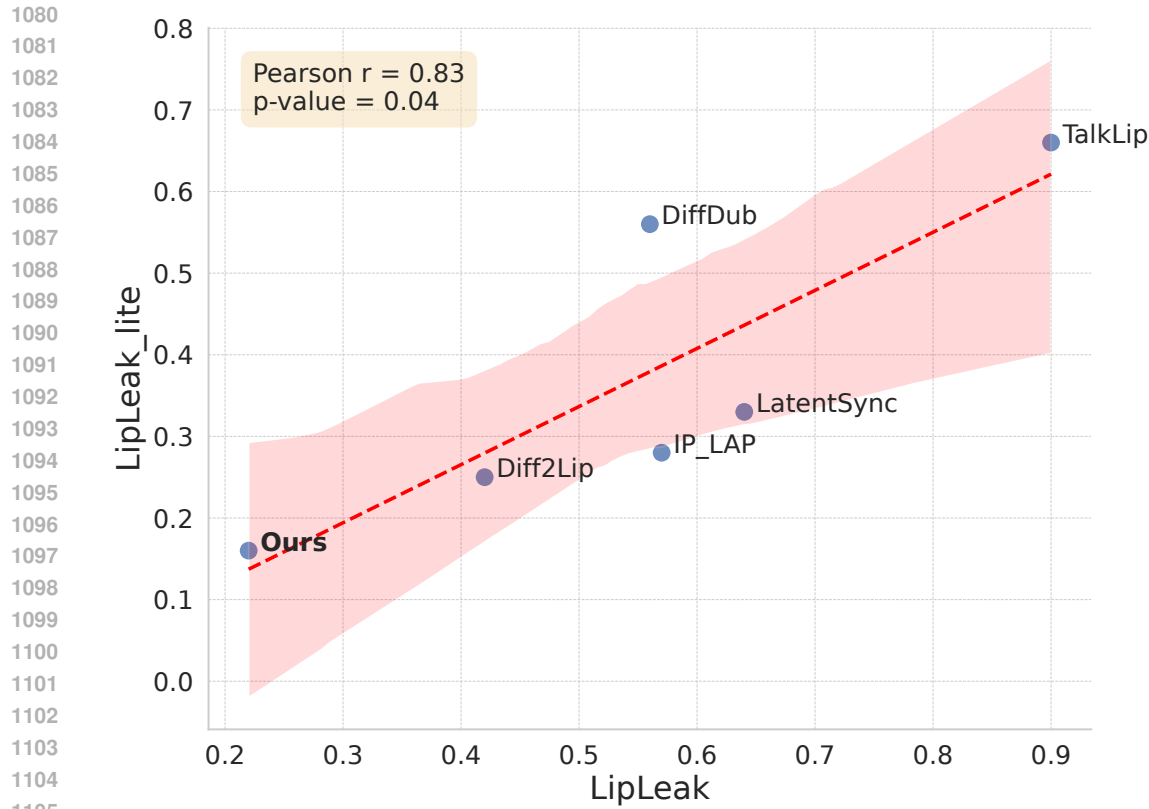


Figure 12: Correlation between Mouth Stability Metrics.

- **TalkLip Wang et al. (2023a):** At first glance, TalkLip appears to function without occlusion handling. However, it achieves this by concatenating frames from the original video to generate new frames. This shortcut enables occlusion handling but comes at the cost of significant expression leakage, as evidenced by its very high LipLeak score in Table 1.



Figure 13: Effectiveness of Occlusion Handling Across Different Methods.

1134 **F USER STUDY RESULTS**

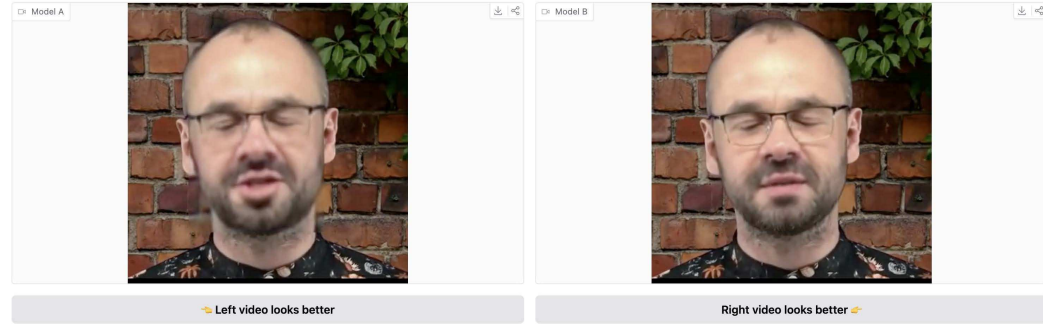
1135
 1136 To ensure that the objective metrics presented in Table 1 align with human perception, we conduct
 1137 a user study to evaluate model performance in terms of lip synchronization, overall coherence, and
 1138 image quality. Participants are presented with pairs of videos and asked to select the one they
 1139 preferred based on these criteria. The video pairs are randomly sampled from the pool of models
 1140 listed in Table 1 to ensure a fair and unbiased comparison. A total of 1,000 pairwise comparisons
 1141 were collected, providing a robust dataset for evaluating human preferences. Figure 14 shows a
 1142 screenshot of the user study interface, illustrating the evaluation setup.

1143
 1144 **Welcome to the Dubbing Evaluation Arena!**
 1145 In this study, the models modify only the lip region of the characters to better match the new dubbed audio, while the rest of the video remains unchanged.
 1146 Please compare the two videos and vote for the one you prefer based on the following criteria:
 1147

- **Lip Synchronization with Audio:** How well the character's lip movements align with the new speech.
- **Overall Coherence:** How seamlessly the modified lip movements integrate with the rest of the video.
- **Image Quality:** Clarity and visual appeal of the video.

 1148 Select either the left or right video as your preference. Thank you for your feedback!

1149 **(Note: If you are on a mobile phone, try turning the screen landscape for a better experience)**



1150
 1151 Figure 14: User study interface. Participants were shown side-by-side videos and asked to select the
 1152 preferred one based on lip synchronization, coherence, and quality.
 1153
 1154
 1155
 1156
 1157
 1158

1159
 1160 **Elo Ratings** To assess the relative performance of different models in our evaluation framework,
 1161 we employ the Elo rating system Elo (1978), a widely used method for ranking competitors based on
 1162 pairwise comparisons. The Elo rating system assigns scores to models based on their performance
 1163 in direct comparisons, updating their ratings dynamically as more results are collected.

1164 We evaluate Elo ratings in two distinct settings:

1165
 1166

- **Reconstruction setting (Figure 15):** In this scenario, we compare videos generated
 1167 using the same audio as in the original video.
- **Cross-Synchronization Setting (Figure 16):** In this scenario, we compare videos generated
 1168 using a different audio from the original video.

1169
 1170 In both cases, our model consistently outperforms competing methods, achieving higher Elo rat-
 1171 ings. This demonstrates its superior ability to generate high-quality, accurately synchronised lip
 1172 movements, both in the reconstruction and cross-synchronization tasks.
 1173

1174
 1175 **Elo Rating Distributions** To better understand the distribution and variance of model rankings,
 1176 we analyse the overall Elo ratings across all evaluated models. Figure 17 presents a histogram of
 1177 Elo scores, illustrating how models are ranked relative to each other. A well-separated distribu-
 1178 tion suggests clear performance differences between models, whereas overlapping scores indicate
 1179 models with similar performance levels. Our model achieves the highest Elo ratings, forming a well-
 1180 defined peak that highlights its superior performance. In contrast, baseline models display varying
 1181 degrees of separation, with some exhibiting significant overlap, suggesting closer competition and
 1182 comparable performance in certain cases.
 1183

1184
 1185 **Win Rates** Beyond Elo ratings, we compute win rates to assess how often each model outperforms
 1186 others in pairwise comparisons. The win rate matrix in Figure 18 provides a detailed overview

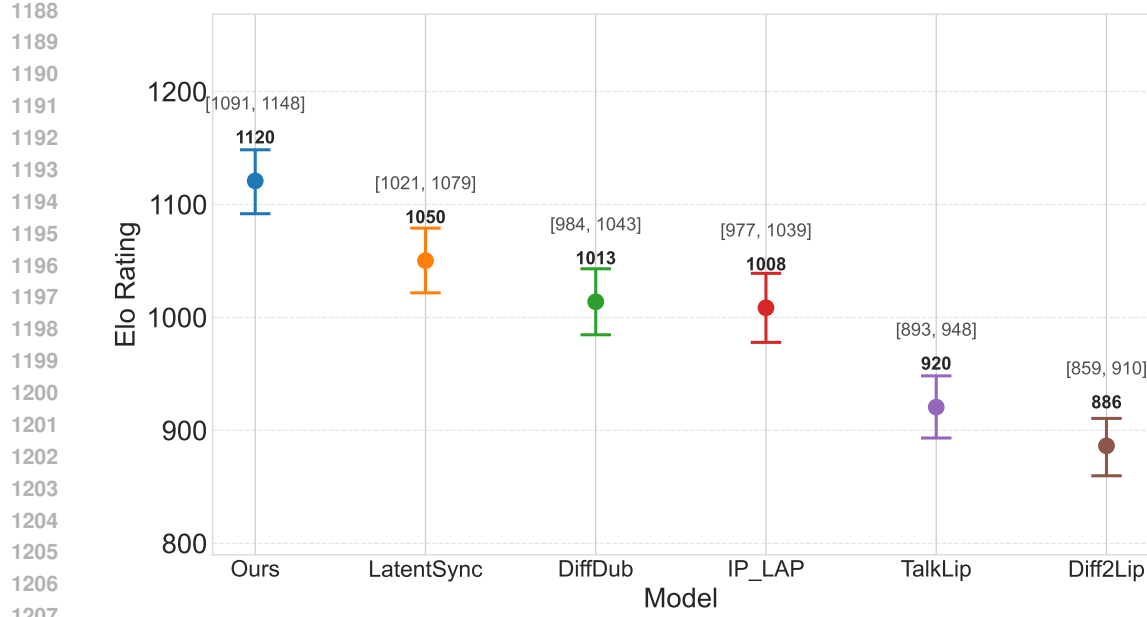


Figure 15: Elo ratings in the reconstruction setting. Higher ratings indicate better performance in generating videos with original audio as input.

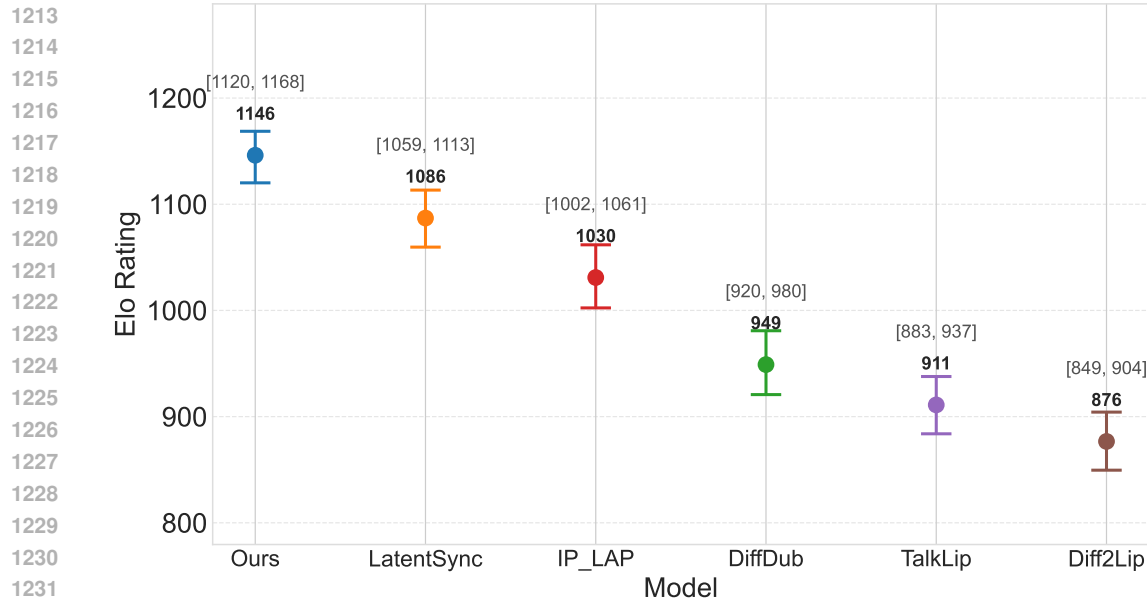


Figure 16: Elo ratings in the cross-sync setting. Higher ratings indicate better performance in generating videos with different audio from input.

of direct matchups, where each cell represents the percentage of times one model wins against another. This analysis helps identify dominant models and potential inconsistencies in ranking. Our model consistently outperforms competing approaches, achieving a minimum win rate of 69 % and a maximum of 94 %. These results indicate a strong and reliable performance advantage over alternative methods.

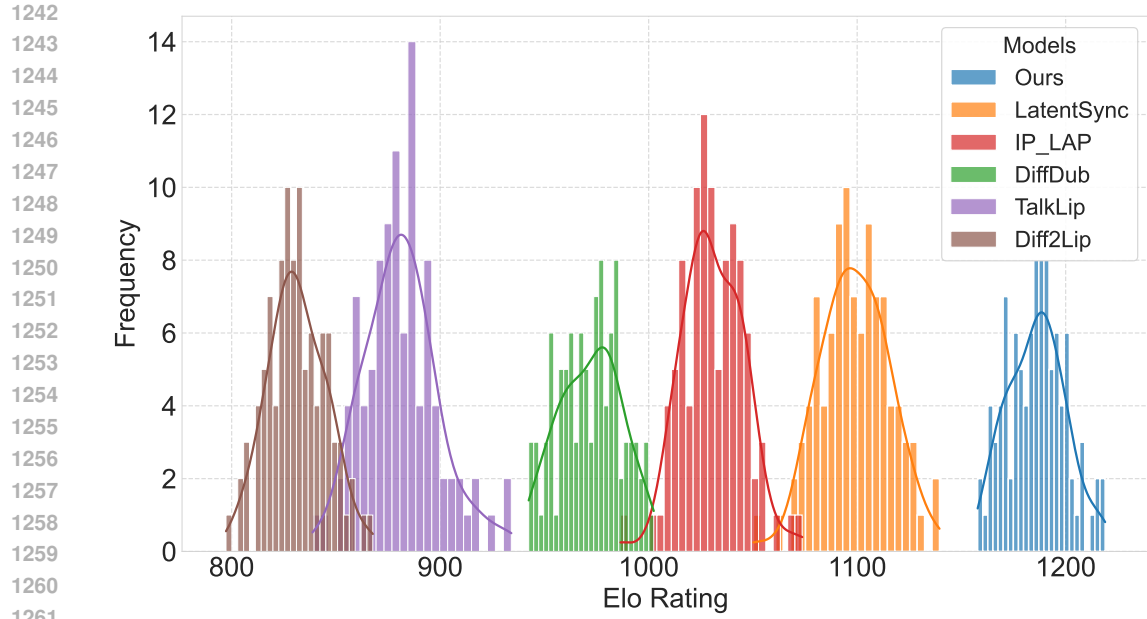


Figure 17: Distribution of Elo ratings across all evaluated models. This histogram illustrates the spread of Elo scores, highlighting performance gaps or clustering amongst different models.

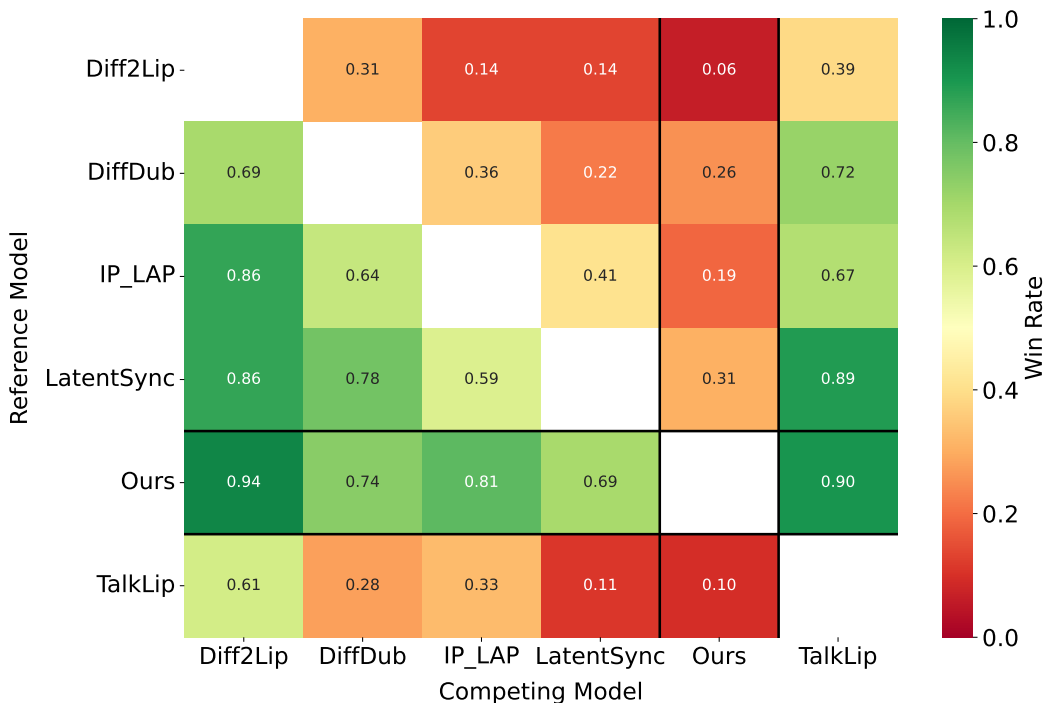


Figure 18: Win rate matrix for pairwise model comparisons. Each cell represents the proportion of matchups where one model outperforms another, offering insight into head-to-head performance.

1296 **G ADDITIONAL RESULTS**
12971298 **G.1 ADDITIONAL BASELINES**
12991300 In Section 5, we compare our method with five strong baselines. We also ran additional experiments
1301 against Wav2Lip Prajwal et al. (2020), due to its position as a foundational lip synchronization
1302 model, and VideoReTalking Cheng et al. (2022), as it also attempts to mitigate expression leakage.
1303 We present the results in Table 9. We observe that while VideoReTalking reduces leakage more
1304 effectively than Wav2Lip, its performance on cross-driving synchronization is still poor.

Method	CMMD \downarrow	TOPIQ \uparrow	VL \uparrow	FVD \downarrow	LipScore \uparrow	LipLeak \downarrow
Reconstruction						
VideoReTalking Cheng et al. (2022)	0.263	0.45	29.28	536.12	0.45	-
Wav2Lip Prajwal et al. (2020)	0.201	0.44	27.59	506.41	0.48	-
KeySync	0.064	0.58	70.32	191.21	0.46	-
Cross-synchronization						
VideoReTalking Cheng et al. (2022)	0.329	0.38	13.03	507.85	0.26	0.42
Wav2Lip Prajwal et al. (2020)	0.205	0.45	27.70	562.63	0.22	0.71
KeySync	0.070	0.58	73.04	206.32	0.48	0.22

1316 Table 9: Additional quantitative comparison.
13171318 **G.2 ADDITIONAL SYNCHRONISATION METRICS**
13191320 While not included in our main comparison (Table 1) due to their known flaws, we present additional
1321 results using the Lip-Sync Error Confidence (LSE-C) and Lip-Sync Error Distance (LSE-D) metrics
1322 from SyncNet Chung & Zisserman (2016). Despite their limitations, these metrics remain widely
1323 used. The results for all baselines are shown in Table 10.

Metric	DiffDub	IP_LAP	Diff2Lip	TalkLip	LatentSync	VideoReTalking	Wav2Lip	KeySync
LSE-D \downarrow	14.59	9.78	7.44	9.52	7.66	9.47	8.04	7.31
LSE-C \uparrow	0.67	4.17	7.10	4.85	7.35	5.79	6.55	7.88

1328 Table 10: Additional quantitative metrics using SyncNet.
13291331 **H ADDITIONAL ABLATIONS**
13321334 **Guidance** Guidance plays a crucial role in the performance of diffusion models Dhariwal &
1335 Nichol (2021); Ho et al. (2020). In our case, we use a modified version of Classifier-Free Guid-
1336 ance (CFG) Ho (2022), which applies separate scaling factors to the audio and identity conditions.
1337 Specifically, our guidance function is defined as follows:

1338
$$z = z_\emptyset + w_{\text{id}} \cdot (z_{\text{id}} - z_\emptyset) + w_{\text{aud}} \cdot (z_{\text{id} \& \text{aud}} - z_{\text{id}}), \quad (9)$$

1339

1340 where:

1341

- 1342 • w_{aud} and w_{id} are the guidance scales for audio and identity, respectively.
- 1343 • z_\emptyset represents the model output when all conditions are set to 0.
- 1344 • z_{id} is the output when only the identity condition is applied.
- 1345 • $z_{\text{id} \& \text{aud}}$ is the output when both audio and identity conditions are applied.

1347 By separating the audio and identity guidance conditions, we enable more control over the generated
1348 videos, ultimately leading to improved performance. Experimentally, we found that setting $w_{\text{aud}} = 5$
1349 and $w_{\text{id}} = 2$ yields the best results. This configuration achieves a 29.73 % improvement in LipScore,
significantly enhancing lip synchronization accuracy. While this comes at a 14.75 % increase in

1350
 1351 CMMMD and a minor 2.80 % increase in FVD, the overall perceptual quality remains strong, making
 1352 this trade-off highly beneficial for generating realistic and synchronized videos. We summarize these
 1353 results in Table 11, demonstrating the effectiveness of our approach compared to standard CFG.
 1354

Guidance	CMMMD ↓	FVD ↓	LipScore ↑
CFG	0.061	200.71	0.37
Ours ($w_{\text{aud}} = 5, w_{\text{id}} = 2$)	0.070	206.32	0.48

1358 Table 11: Guidance ablation in the cross-sync setting.
 1359
 1360

1361 **Losses** We present an ablation on the impact of applying a pixel loss in addition to the diffusion
 1362 loss in Table 12. Our findings indicate that adding a L_2 loss in pixel space leads to a slight improve-
 1363 ment in image and video quality while maintaining the same level of lip synchroniza-
 1364 tion. However, contrary to the findings in Bigata et al. (2025), we did not find that adding an additional LPIPS
 1365 pixel loss benefits the model. Instead, it causes the mouth region to deviate too much from the rest of the
 1366 image, as illustrated in Figure 19. This discrepancy arises because facial animation is a different
 1367 task from lip synchronization, with the latter being more closely related to an inpainting task rather
 1368 than full facial reconstruction.
 1369

Loss	CMMMD ↓	FVD ↓	LipScore ↑
No pixel loss	0.075	215.71	0.48
L_2	0.070	206.32	0.48

1374 Table 12: Pixel loss ablation in the cross-sync setting.
 1375
 13761377 Figure 19: Examples of inconsistent mouth regions obtained by training with an additional LPIPS
 1378 pixel loss.
 1379
 13801381

I LIMITATIONS

 1382

1383 To assess the limitations of our approach, we construct a small dataset consisting of seven identities,
 1384 where each individual recites the same two sentences at five different angles: 0°, 20°, 45°, 70°,
 1385 and 90°, as illustrated in Figure 21. This setup allows us to systematically evaluate how the model
 1386 performs under varying viewpoint conditions.
 1387

1388 We present the results of TOPIQ Chen et al. (2024a) with respect to the angle in Figure 20. We use
 1389 TOPIQ because it is a no-reference image quality metric that does not require a large ground-truth
 1390 dataset for direct comparison, making it more practical than FID or FVD, which rely on reference
 1391 distributions that may be skewed or incomplete across extreme angles. Additionally, unlike variance
 1392 of Laplacian (VL), which only captures blurriness, TOPIQ provides a more comprehensive measure
 1393 of perceptual quality degradation, including semantic distortions that become more pronounced at
 1394 oblique head poses. The results indicate that all approaches exhibit performance degradation as the
 1395 angle increases. This is a key limitation of our model, which is also observed across baseline meth-
 1396 ods. This decline in performance can be attributed to the inherent biases in our training datasets,
 1397 which predominantly contain frontal faces. As a result, the model struggles to infer occluded or
 1398 unseen facial regions when presented with extreme head poses. One potential solution is to provide
 1399

identity frames from multiple viewpoints during training, allowing the model to learn a more comprehensive facial representation. However, this would require extensive new data collection and further investigation, and is therefore left for future work.

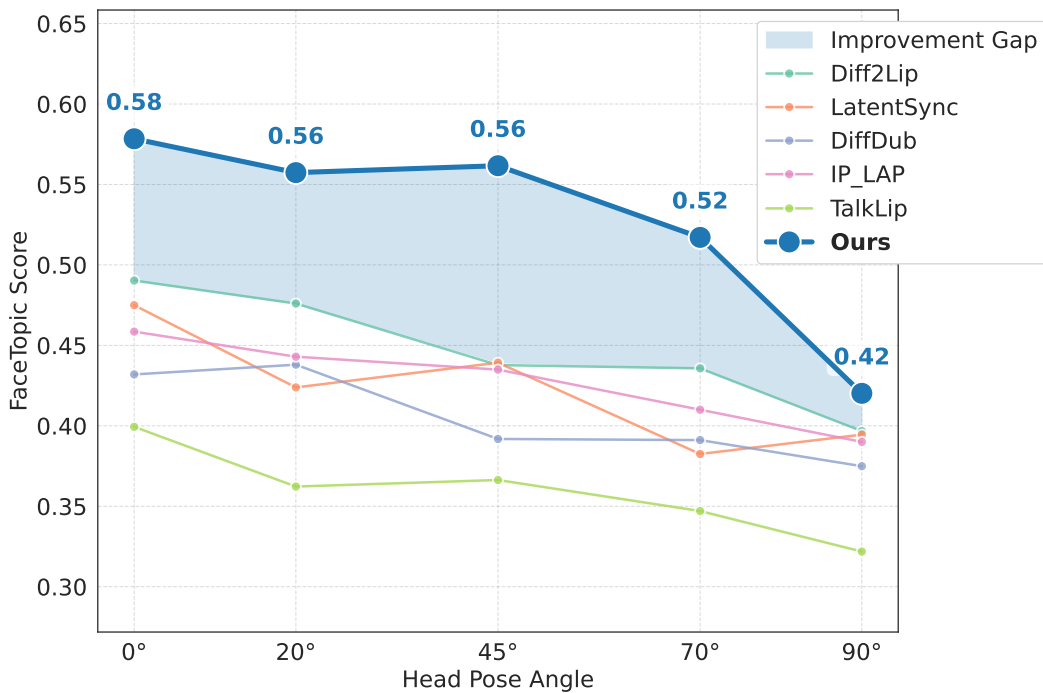


Figure 20: Impact of head pose on model performance.



Figure 21: Examples of generated videos at different angles.

J ADDITIONAL QUALITATIVE RESULTS

We present additional qualitative results in Figure 22. As reported in the main paper, our model demonstrates better alignment with the target lips while also achieving higher image quality compared to other methods. Additionally, we evaluate our model’s ability to handle non-human faces in Figure 23. We find that KeySync produces plausible lip-synced animations, while competing models fail to accurately reconstruct mouth details, particularly in the first two identities, as they deviate significantly from typical human facial structures. This highlights our model’s superior adaptability in handling out-of-distribution (OOD) scenarios.

To better assess the effectiveness of our approach, we provide a series of videos as part of the supplementary material. These videos are categorized as follows:

- **Side-by-side comparisons:** Showcasing our method against other approaches in both reconstruction and cross-sync settings.
- **Silent videos:** Highlighting expression leakage within the same video, demonstrating how different models handle silent audio.

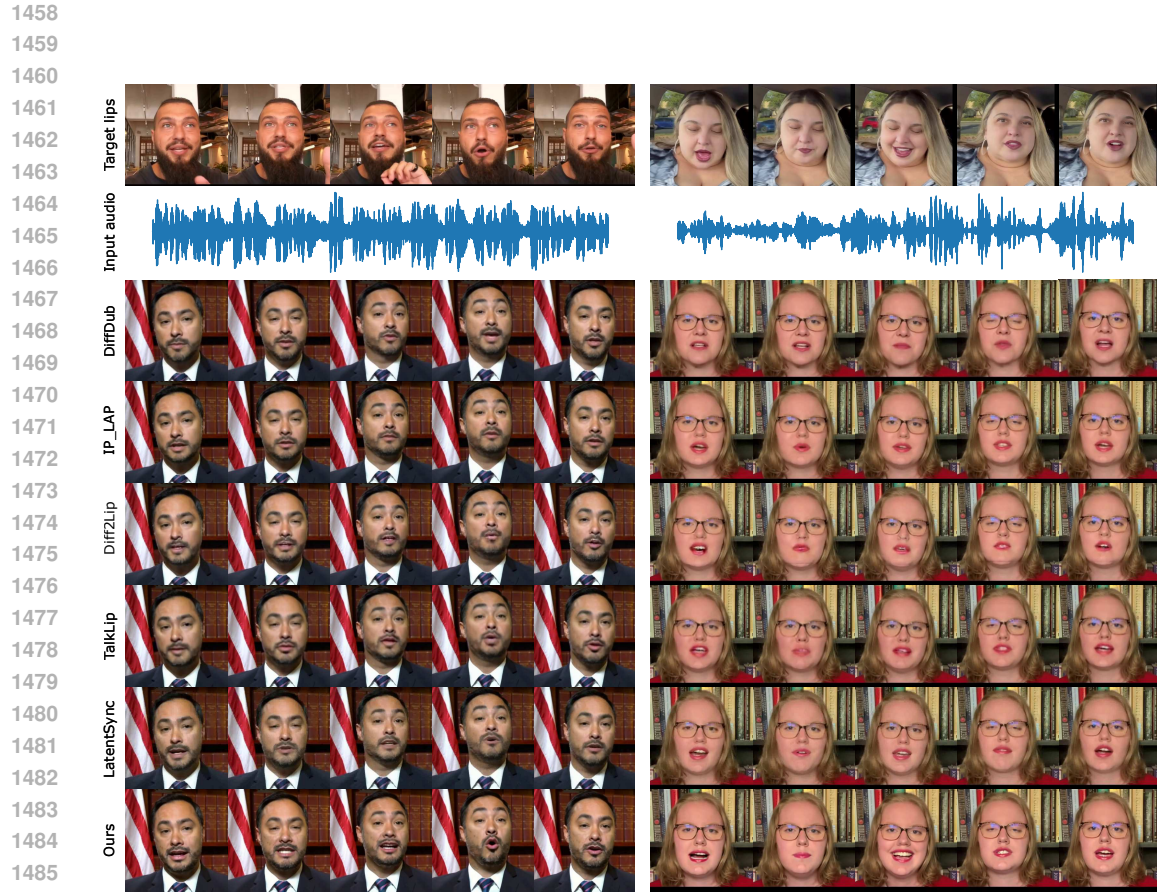


Figure 22: Additional qualitative comparison.



Figure 23: Qualitative comparison on non-human ids.

- 1512 • **Occlusion cases:** Also included in the same video, presenting situations where parts of the
1513 face are obstructed, illustrating the robustness of our approach.
- 1514 • **Multilingual examples:** Evaluating the model’s performance across different languages to
1515 assess generalization.
- 1516 • **Out-of-distribution examples:** Testing our model on non-human identities, demonstrating
1517 its adaptability to non-human faces.
- 1518 • **Examples at different angles:** Analyzing the model’s performance under varying head
1519 poses, highlighting its ability to handle different viewpoints as well as its limitations.
- 1520 • **Additional cross-sync videos:** Providing a more extensive evaluation of our model’s cross-
1521 sync capabilities across various conditions.

1523
1524 These supplementary videos offer a comprehensive visual demonstration of our method’s perfor-
1525 mance across a wide range of conditions.

1526 K ETHICAL CONSIDERATIONS AND SOCIAL IMPACT

1529 **User study** Our study includes a user evaluation where participants compare video outputs for
1530 lip synchronization, image quality, and coherence. All participants provided informed consent, and
1531 their responses were collected anonymously. No personally identifiable information or sensitive data
1532 were gathered, ensuring compliance with ethical research guidelines.

1533 **Model** Lip-sync generation has numerous beneficial applications, including enhanced video dub-
1534 bing, accessibility tools for hearing-impaired individuals, and improvements in digital content cre-
1535 ation. However, we acknowledge that such technology can also be misused, particularly in the
1536 context of deepfake generation, which poses risks related to misinformation, identity fraud, and
1537 unethical content manipulation. To mitigate potential misuse, we emphasize that our approach is
1538 developed with a focus on fair use cases and is intended strictly for research purposes.

1540 **Datasets** We rely on publicly available datasets that were originally collected and published by
1541 external researchers. We adhere to the terms and ethical guidelines set by the dataset creators.

1543 L USE OF LARGE LANGUAGE MODELS

1545 During the preparation of this manuscript, we utilized a Large Language Model (LLM), specifically
1546 Gemini, to assist with language editing. The LLM’s role was strictly limited to proofreading for
1547 grammatical errors and improving the clarity and conciseness of sentences. All content, including
1548 the research ideas, methodology, results, and conclusions, was conceived and written by the human
1549 authors. The authors reviewed and edited all LLM-generated suggestions and take full responsibility
1550 for the final content of this paper.